Summer 2018

Daytime Summer Microclimate Influence of Large Woody Debris on Dewatered Sediments in Lake Mills, WA Following Dam Removal

Mariah J. Colton
Western Washington University, mariah.colton@gmail.com

Daytime Summer Microclimate Influence of Large Woody Debris on Dewatered Sediments in Lake Mills, WA Following Dam Removal

By

Mariah J. Colton

Accepted in Partial Completion

of the Requirements for the Degree

Master of Science

ADVISORY COMMITTEE

Chair, Dr. Peter S. Homann

Dr. Andy Bach

Dr. James Helfield

GRADUATE SCHOOL

Gautam Pillay, Dean

Master's Thesis

In presenting this thesis in partial fulfillment of the requirements for a master's degree at Western Washington University, I grant to Western Washington University the non-exclusive royalty-free right to archive, reproduce, distribute, and display the thesis in any and all forms, including electronic format, via any digital library mechanisms maintained by WWU.

I represent and warrant this is my original work, and does not infringe or violate any rights of others. I warrant that I have obtained written permissions from the owner of any third party copyrighted material included in these files.

I acknowledge that I retain ownership rights to the copyright of this work, including but not limited to the right to use all or part of this work in future works, such as articles or books.

Library users are granted permission for individual, research and non-commercial reproduction of this work for educational purposes only. Any further digital posting of this document requires specific permission from the author.

Any copying or publication of this thesis for commercial purposes, or for financial gain, is not allowed without my written permission.

Mariah J. Colton

May 30, 2018

Daytime Summer Microclimate Influence of Large Woody Debris on Dewatered Sediments in Lake Mills, WA Following Dam Removal

A Thesis

Presented to

The Faculty of

Western Washington University

In Partial Fulfillment

Of the Requirements for the Degree

Master of Science

by Mariah J. Colton

June 2018

Abstract

In 2014, dam removal from the Elwha River, Washington state, exposed large areas of previously submerged sediment. The Olympic National Park placed 100 large logs on 2 ha of exposed sediment to promote plant establishment. I quantified patterns of three microclimate variables near logs: wind speed at 10-cm height (u_{10}), sediment temperature (T_S), and evaporation rate (E); and their relationships to broader environmental factors. The northern-most log, exposed to northerly winds, was measured along 3-m perpendicular transects 14 times during August and September 2015. I determined nonlinear and multilevel regressions to investigate patterns and create models of microclimate as functions of environmental factors and distance from the log. Maximum u_{10} decreased to the lee. Decreases near the log occurred for u_{10} to the north and south, and for T_S and E to the shaded north. Windward and leeward u_{10} models include local wind speed and distance from log. Northern T_S is related to solar radiation, air temperature and distance from log. Southern T_S is related to air temperature. Northern E is related to solar radiation, vapor pressure deficit and distance from log. Southern E is related to solar radiation and vapor pressure deficit. Models of southern u_{10} and northern T_S and E were validated with data from 8 wind-protected logs, but lack of validation of the other microclimate models indicate the northern-most log has unique microclimate. Species-specific physiological information is required to predict plant reactions to near-log microclimate. All models require more data to broaden their scope.

Acknowledgments

I would like to thank my thesis advisor, Dr. Peter Homann for his valuable support throughout this research and my thesis committee, Dr. Andy Bach and Dr. James Helfield for their expertise and advice.

I would also like to thank Olympic National Park and Jerry Freilich for allowing me to conduct my research in Lake Mills and for undergoing this restoration project to provide critical information on dam removal restoration. Thank you to Josh Chenoweth and Bill Baccus for providing critical information on the Lake Mills site, including the log-drop area studied in this thesis and for providing weather data. Thank you also to Nancy Bluestein-Johnson and Huxley on the Peninsulas for providing a workspace in Port Angeles during field sample collection. And thanks to Gay Hunter and David Henning for generously providing housing in Port Angeles during field sampling.

Thanks also to my parents and sister, whose support throughout this project was essential to completing it.

And lastly, I must express my gratitude for the help of my husband and field assistant, Jake Clemens, for giving me constant support throughout the brutally hot summer of sampling in Lake Mills and the many more hours spent putting this document together.

Contents

List of Figures

List of Tables

List of Symbols

u	wind speed
u_{10}	wind speed at 10 cm height
$\bar{u}_{100}$	average wind speed at 100 cm height
z_0	roughness distance
z	height from sediment surface
d	distance from log edge, either north or south
R_{at}	thermal radiation from atmosphere
R_{Sdiff}	diffuse solar radiation
R_{SD}	direct solar radiation
R_{rsw}	reflected shortwave radiation
R_{gt}	emitted thermal radiation from the ground surface
Q_s	sensible heat transfer to soil or sediment
T_S	sediment temperature
T_a	air temperature
$R_{S,2h}$	two-hour cumulative solar radiation
$R_{S,4h}$	four-hour cumulative solar radiation
R_S	one-hour average solar radiation
ρ	vapor pressure deficit
P_w	partial pressure of water vapor
E	evaporation rate

Chapter 1

Introduction

1.1 Background

Dam removal is becoming a prevalent strategy for restoring river ecosystems and aging-dam management (Stanley and Doyle, 2003; American Rivers, 2014). As this trend continues, knowledge on how to recover from dam removal will be essential. However, dam removal strategies and post dam removal recovery strategies are variable and not well researched (Stanford et al., 1996; Tullos et al., 2016; Bellmore et al., 2017). Two hydroelectric dams were recently removed on the Elwha River, Washington: The 87 year old Glines Canyon Dam, which impounded Lake Mills reservoir and the 99 year old Elwha Dam, which impounded Lake Aldwell reservoir (Winter and Crain, 2008; Chenoweth et al., 2011). As a result of the removal of the two dams, approximately 3.2 square kilometers of sediment were exposed. Revegetation of these reservoir sediments is a critical aspect of the Elwha River restoration for promoting adequate salmon habitats and maintaining ecosystem function.

The Pacific Northwest has characteristically wet winters and warm, dry summers that bring drought stress to vegetation during the growing season (Waring and Franklin, 1979; Gray and Spies, 1997). Less than 10% of annual precipitation falls during the summer months (Waring and Franklin, 1979). Additionally, water availability in the sediments is expected to be low due to the small pore spaces of the

sediments (Niinemets, 2010; Chenoweth et al., 2011). Therefore, microclimate of the exposed reservoir sediments may not be adequate for natural seed germination and growth on the Elwha River without some manipulation (Michel et al., 2011).

Olympic National Park has a management and monitoring plan in place to promote revegetation (Chenoweth et al., 2011). One aspect of this plan is the placement of large woody debris (LWD) on exposed sediment surfaces to provide refuge from herbivory, provide shade and reduce moisture stress to establishing vegetation (McHenry and Chenoweth, 2015). In 2012 and 2014, large logs were placed on the exposed sediments of former Lake Mills by helicopter to assist vegetation, but it remains unknown how these logs may be affecting their surrounding microclimate, which ultimately influences the vegetation (Chen et al., 1995; Gray and Spies, 1997; Chenoweth et al., 2011; Jones, 2013; McHenry and Chenoweth, 2015).

The purpose of this study is to determine the spatial and temporal patterns of microclimate near placed LWD and to determine how external weather phenomena influence the effect that logs have on the surrounding microclimate.

1.2 Microclimate Conceptual Models

1.2.1 Microclimate Definition and Scope

Microclimate is officially defined in climatology and meteorology as the climatic region in the air space near the ground surface, up to 1.5 or 2 meters high (Ahrens, 2005; Geiger et al., 2009). However, the term microclimate is also frequently used to describe the below ground environment in soils and sediments (Harte et al., 1995; Raich and Tufekciogul, 2000; Jo et al., 2017). Microclimate often describes the localized area of climate experienced by an organism or community in question and may differ from the surrounding climate, allowing the organism or community to survive (Middleton, 1999; Middleton, B., 2000; Blood and Titus, 2010). It is a result of many environmental factors in an ecosystem, including the biological, hydrological, biophysical and topographical. Microclimate has both a direct and an indirect

effect on all ecosystem processes and these ecosystem processes also strongly affect the microclimate. Topography and vegetation are important drivers of microclimate because they cause heterogeneity of energy and water balance in a landscape and therefore microclimate is often distinct in different landscape patches (Chen et al., 1999; Xu et al., 2004).

Climatic conditions vary greatly based on distance above the ground and can also vary greatly based on horizontal distance (Rosenberg et al., 1983; Ahrens, 2005; Likso and Pandžić, 2006; Geiger et al., 2009). Likso and Pandžić (2006) observed diurnal temperature variation at 5 cm height to be between 2 ^{o}C and 5 ^{o}C greater than the diurnal temperature variation at 2 m height, depending on the season. Davies-Colley et al. (2000) observed differences in microclimate across a forest-pasture edge. They reported an abrupt 5 ^{o}C drop in soil temperature over a horizontal distance of 10 meters, and drops in wind speed (1.25 m/s difference), air temperature (6 ^{o}C difference) and vapor pressure deficit (4.5 mB difference) over a 40 meter distance. Other studies show similar changes in climatic variables over similar distances (Gehlhausen et al., 2000; Newmark, 2001).

The terms and concepts of microclimatology are based on physics and physical relationships (Geiger et al., 2009). Microclimate can be described by physically derived variables related to localized energy and water budgets, such as temperature, heat, radiation, evaporation and wind speed, among others (Rosenberg et al., 1983; Geiger et al., 2009; Jones, 2013). All variables are intrinsically related and relationships can be defined by mathematical models (Rosenberg et al., 1983; Jones, 2013).

1.2.2 Wind Speed (u)

The microclimate-relevant layers of the atmosphere are the laminar sublayer and the turbulent surface layer (Rosenberg et al., 1983). The laminar sublayer extends only a few millimeters above the ground surface and mass and energy transfers here are due mainly to molecular diffusion. The turbulent surface layer then extends above the laminar sublayer up to 50 – 100 meters. This layer is characterized by strong

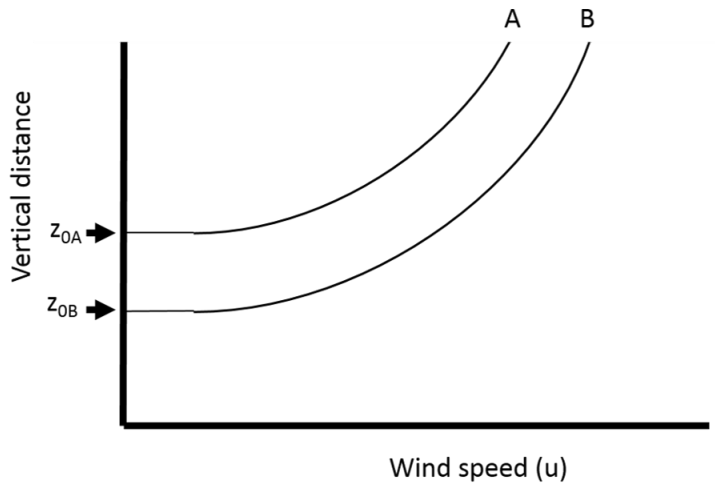

Figure 1.1: Separate wind profiles A and B are described by differences in the patterns of wind speed at varying vertical distance or height above the ground surface. Wind profile A has a roughness distance (z_0) value of z_{0A} and wind profile B has a roughness distance of z_{0B}. Roughness distance describes the height at which wind speed becomes negligible and is used to compare different ground surface types and how they affect wind profiles. At greater vertical distances, the wind follows a logarithmic curve as described in log wind profile models, offset by their z_0 intercepts. Roughness distance is explained further in Appendix B.

eddying and mixing due to surface friction (mechanical turbulence), and temperature gradients and convection (thermal turbulence) (Rosenberg et al., 1983).

Wind speed (u) decreases with proximity to the ground, due to friction caused by surface roughness (Rosenberg et al., 1983; Geiger et al., 2009). There are several mathematical models that use the differences in u at different heights to characterize a surface's influence on wind (Swinbank, 1964; Tennekes, 1973; Rosenberg et al., 1983; Geiger et al., 2009; Jones, 2013). Several models show u proportional to the natural log of the height above the ground (Swinbank, 1964; Tennekes, 1973; Rosenberg et al., 1983; Jones, 2013). Figure 1.1 outlines the basic profile described in one of these models. These wind-profile models are typically applied on a meter to kilometer scale, but can mathematically be applied to a centimeter spatial scale to describe microclimatatological and micrometeorological patterns.

1.2.3 Sediment Temperature (T_S)

Sediment temperature (T_S) is the sensible heat in and below the sediment surface caused by solar radiation and thermal conductivity (Rosenberg et al., 1983). Incident solar radiation (R_S) is the primary controller of energy input into soil, microclimate systems and to the global energy budget (Rosenberg et al., 1983; Geiger et al., 2009). Incident solar radiation includes both direct solar radiation (R_{SD}) from outside of the atmosphere and diffuse solar radiation (R_{Sdiff}) (Figure 1.2). Direct solar radiation is the direct beam of light from the sun that is not scattered by atmospheric particles (Jones, 2013). The amount of direct solar radiation that reaches earth surfaces depends heavily on water vapor or particulate matter content in the atmosphere, latitude, season and diurnal sun position. Diffuse radiation is the solar radiation that is transmitted to the ground surface due to scatter from atmospheric particles. In mid-latitudes, diffuse solar radiation can input 30-40% of the incident total solar radiation to the surface and is a greater portion of the total solar radiation when there is increased cloud cover or during winter months (Rosenberg et al., 1983). Some heat absorbed from radiation in the atmosphere is also emitted towards the earth surface (R_{at}).

Once at the ground surface, the radiation not absorbed as Q_s is either reflected as shortwave radiation (R_{rsw}) or emitted as thermal (longwave) radiation (R_{gt}) (Rosenberg et al., 1983). The R_{rsw} is incident solar radiation reflected from surfaces in the 0.3-0.7 μm wavelengths, which includes both shortwave and visible wavelengths of the spectrum. The R_{rsw} is sometimes also termed 'albedo'. Rocky, sandy and bare soil surfaces reflect 10-30% of incident shortwave solar radiation, while water reflects very little and absorbs a majority of solar energy. The R_{gt} is the net upward longwave radiation given off by on an object and is dependent on its temperature (Jones, 2013). Both the atmosphere and land surface emit longwave radiation and the net difference between downward and upward longwave radiation emitted from the land surface is noted as the net upward longwave radiation.

While some incoming radiation is reflected in short and longwave radiation, soil

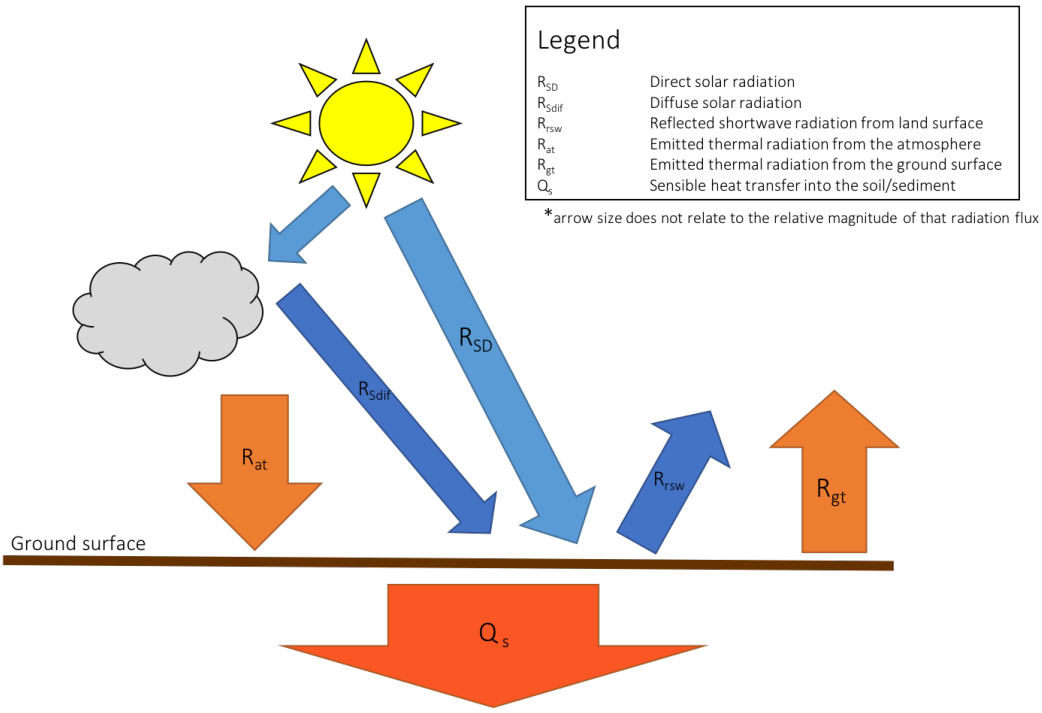

Figure 1.2: Radiation balance at the ground surface is depicted showing radiation and heat fluxes within a simple ground surface. The incoming radiation variables are emitted thermal radiation from the atmosphere (R_{at}), direct solar radiation (R_{SD}) and diffuse solar radiation (R_{Sdiff}). Direct and diffuse solar radiation are both components of the total incoming solar radiation (R_S). The incoming energy is then transferred to the soil as sensible heat (Q_s) and is reflected as shortwave radiation (R_{rsw}). Additionally, the temperature of the soil causes it to emit thermal energy back to the atmosphere (R_{gt}).

and sediment surfaces also absorb the light energy. These surface types are highly important in heat storage on virtually all spatial and time scales (Rosenberg et al., 1983). Generally, soil temperature changes with depth. This profile changes as incoming radiation is absorbed, heat is conducted through the soil or sediment and longwave radiation is emitted from the ground surface (Rosenberg et al., 1983). Soil and sediment temperature decreases with depth during the day and the temperature gradient causes heat to go into the soil or sediment. Heat that is transferred due to temperature difference is termed sensible heat (Q_s). Sandy soils experience greater extremes of temperatures diurnally due to lower heat capacity and greater thermal conductivity due to smaller pore space - assuming equal water content. Additionally, differences in temperature can cause differences in water distribution within the soil, both liquid and vapor. This is a consequence of the upward and downward conductivity of thermal energy diurnally within the soil causing differences in water vapor pressure (Rosenberg et al., 1983).

Heat from the ground surface is also conducted upward to atmospheric gases and particles near the ground surface (Rosenberg et al., 1983; Shuttleworth, 1993). The magnitude of this vertical flux of sensible heat from the ground to the atmosphere (R_{gt}) is primarily dependent on the difference in temperature for the first 2-3 meters above the ground and the direction of the flux is dependent on the time of day (Rosenberg et al., 1983; Shuttleworth, 1993). When the surface is warmer than the air, during the day, the flux is upward. When the surface is cooler, which may occur at night, sensible heat is transferred from the atmosphere to the ground surface (Rosenberg et al., 1983).

1.2.4 Evaporation Rate (E)

Evaporation is the change of state from liquid water to water vapor. Its rate (E) is dependent on energy availability at the surface, the ease of diffusion of water from the surface to the air, and how much water is available at the surface for evaporation (Penman, 1948; Rosenberg et al., 1983; Shuttleworth, 1993). To quantify the

energy available for evaporation from a sediment surface, a radiation balance must be estimated as described in Section 1.2.3, including sensible heat loss to the sediment and nearby air and energy loss via evaporation due to heat of vaporization of water (Penman, 1948; Rosenberg et al., 1983; Shuttleworth, 1993).

The ease of diffusion between the sediment surface and the air is dependent on molecular diffusion and turbulent diffusion (Figure 1.3) (Penman, 1948; Shuttleworth, 1993). Molecular diffusion is a result of a gradient in water vapor partial pressure (called the vapor pressure deficit (ρ)) between the sediment surface and the nearby air (1 to 3 mm thick laminar sublayer) and of constant random motion of air particles (Penman, 1948; Rosenberg et al., 1983; Shuttleworth, 1993). If the relative humidity of the nearby air is fully saturated, evaporation will not occur. Advection aids in molecular diffusion by raising the air close to the sediment surface and replacing it with drier air from above, thereby creating a constant upward movement of water vapor. Turbulent diffusion is advection created by wind-caused turbulence exchanging air close to the sediment surface with air from higher in the atmosphere. The rate at which water vapor is moved from the air close to the sediment surface is proportional to the wind speed and is affected by crops and other objects on the sediment surface that affect wind speeds (Rosenberg et al., 1983; Shuttleworth, 1993). In his foundational equation for evaporation, Penman (1948) described E as directly proportional to wind speed, vapor pressure deficit, and solar radiation. Limiting sediment moisture acts as a resistance to the evaporation rate from bare sediment (Rosenberg et al., 1983; Shuttleworth, 1993).

Plants require ground moisture for transpiration, the water evaporation from stomata in vascular plant leaves. The movement of water through plant tissue from the ground substrate is critical for transport of nutrients and other chemicals through the plant (Jones, 2013). Transpiration is not discernible from evaporation over large areas and thus, these are frequently combined and described as evapotranspiration (Rosenberg et al., 1983; Jones, 2013). Similar factors affect transpiration, but it is also controlled by plant physiology (Jones, 2013).

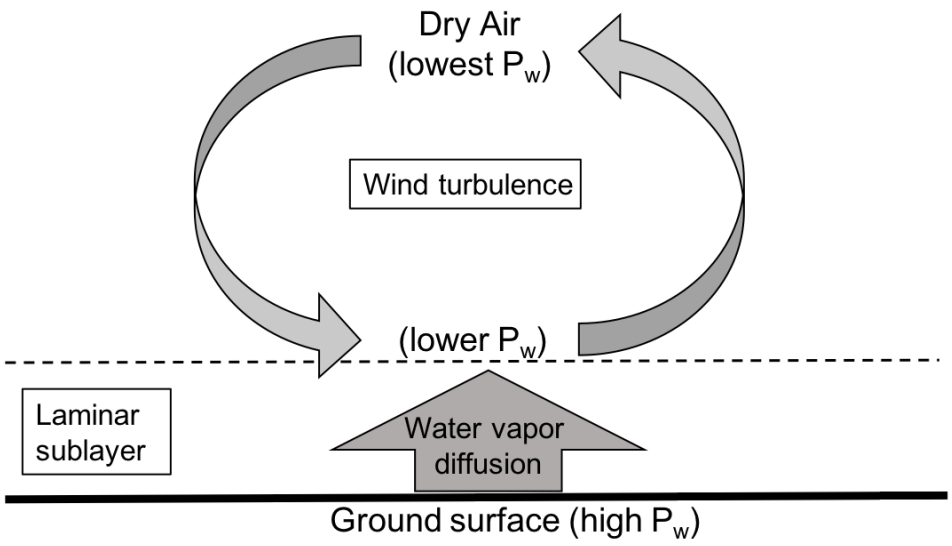

Figure 1.3: Evaporation from the ground to the atmosphere is determined by difference in partial pressure of water vapor (P_w) between the surface and the nearby air. The diffusion of water vapor from the surface to the laminar sublayer is caused by molecular diffusion. From the laminar sublayer to the atmosphere above, the water pressure gradient is influenced by wind turbulence replacing the moist air (greater P_w) near the laminar sublayer with dry air (lesser P_w) from greater heights in the atmosphere.

1.3 Microclimate Influence on Vegetation

The near-ground microclimate layer of the atmosphere is where plants grow and therefore microclimate strongly influences plant life (Rosenberg et al., 1983; Geiger et al., 2009; Jones, 2013). When climatic conditions outside the optimal range of a plant are sustained for long periods of time, plant productivity can be hindered and the climatic conditions are considered a 'stress' (Niinemets, 2010). These climatic conditions can include light availability, moisture availability, temperature and wind speeds (Wadsworth, 1959; Kalma and Kuiper, 1966; Niinemets, 2010). In a study of 806 Northern Hemisphere temperate tree and shrub species, Niinemets and Valladares (2006) found that species are rarely tolerant of two or more environmental stresses. Stress tolerance refers to physiological and/or morphological changes in plants in response to stress to counteract potential decreases in plant productivity and growth (Jones, 2013). This definition is based on the organism level, though some studies have investigated stress tolerance at the community level (Bertness and Callaway,

1994; Lortie and Callaway, 2006; Maestre et al., 2006, 2009; Holmgren and Scheffer, 2010; Butterfield et al., 2016). Specific conditions of microclimate also must exist for seeds to germinate (Middleton, 1999).

Models of microclimate have successfully been used at large scales to predict species survival and growth, where the input variables into the models were climatic variables influential on survival (Kearney and Porter, 2009; Questad et al., 2014). These models are often called species distribution models (SDMs) (Kearney and Porter, 2009). In a review of published SDMs, Kearney and Porter (2009), listed direct and diffuse solar radiation, infrared radiation, air temperature, surface temperature and relative humidity as the important microclimate variables included in SDMs. Questad et al. (2014) created a suitability map using elevation information and compared it to microclimate variables of mean wind speed, soil moisture, relative humidity and air temperature to determine if the suitability map would be accurate in predicting survivorship of at-risk species. Most recently, Kearney and Porter (2017) introduced a microclimate model within the biophysical modelling package NicheMapR, which describes the heat, water and nutritional budgets of organisms partially by inputs of microclimate. The NicheMapR microclimate inputs include mean air temperature, soil moisture, relative humidity, wind speed and cloud cover.

1.3.1 Wind Influences

Plants are subject to damage from winds due to desiccation, chill and mechanical injuries (Grace, 1977; Rosenberg et al., 1983; Grier, 1988). Wind also affects plant morphology and development by reducing leaf area index (LAI) and decreasing total water usage, subsequently reducing growth rate. This is based on experiments done by Wadsworth (1959), Morse and Evans (1962), and Kalma and Kuiper (1966). Grier (1988) found single wind events reduced leaf biomass by 36.3% in conifer forests in the western United States. Kalma and Kuiper (1966) also measured decreases in root and leaf fresh biomass and dry leaf mass with increasing wind speeds between 0 and 1.6 m/s under controlled conditions. Decreased water mass in leaves may

make plants more susceptible to heat stress and evaporative stress (Machado and Paulsen, 2001; Wahid et al., 2007). Wadsworth (1959) found that some wind is beneficial for plant growth and the optimum wind speed is about 0.7 m/s for resulting in the maximum possible growth rate (increase in plant weight per unit weight) of *Brassica napus* (rapeseed) in a controlled laboratory experiment controlling other plant stresses, but this may not apply to other plant species. Increased wind can cause increased evapotranspiration, even when water is limited in the ground (Penman, 1948; Grace, 1977). This causes increased leaf water stress to plants, and in turn, causes drought stress (Grace, 1977). Wind can also stress plants by increasing soil erosion, especially where soils are loose, dry and bare, as is expected with Lake Mills sediments (Fryrear and Skidmore, 1985; Chenoweth et al., 2011).

1.3.2 Sediment Temperature and Energy Influences

Sediment temperature and air temperature are related as described in Section 1.2.3. Where sediment temperatures are elevated, air temperature nearby may also be elevated and vice versa. Elevated temperatures, permanent or transitory can have large negative effects on plant physiology and biochemistry, which affects growth, development and survival at all life stages (Wahid et al., 2007). The temperatures at which these physiological and biochemical changes occur permanently is referred to as 'heat stress'. Heat stress thresholds depend on the intensity of the temperature, how quickly the temperature changes and the duration of exposure of the plant to the increased temperature and is species specific. High temperature can inhibit or slow germination (Covell et al., 1986). Increased temperature can cause leaf senescence, decreased or stopped growth, and plant death (Machado and Paulsen, 2001). Elevated soil temperatures can negatively affect root metabolism and growth, and soil temperature is as important as soil moisture and soil aeration for root health (McMichael and Burke, 1996). In a study of red alder in Pacific Northwest forests, heat and drought injuries were found to be the primary causes of seedling mortality in clearcut areas, where surface organic matter had been removed, exposing mineral

soil (Haeussler et al., 1995). Growth rates in these areas were also slowed. Though this study observed the combined effects of heat and drought stress on red alder, they suggested that temperature variability and daily maximum temperature may have an effect on distribution of red alder, separate from an effect from soil moisture.

1.3.3 Evaporation Influences

Transpiration is critical for transport of nutrients and other chemicals in plants and is therefore essential to plant survival (Jones, 2013). When moisture is limited in the ground substrate, as is likely in Lake Mills (Chenoweth et al., 2011), plants may experience drought stress because transpiration is hindered (Jones, 1999). Low water content in soils can also hinder seed germination (Jajarmi, 2009).

High temperature and drought stress can interact to affect the soil water content, leaf water content and leaf osmotic potential (Machado and Paulsen, 2001). These stresses are derived from decreased soil water, but do not affect physiological changes in the plant such as osmotic adjustment. Water availability and drought stress are often dictators of plant phenology as well (Idso et al., 1978; Aronson et al., 1992).

Haeussler et al. (1995) found that increased soil moisture increased red alder (*Alnus rubra*) emergence in a field experiment in the central Coast Range of Oregon, independent of soil type. ONP conducted a similar study in a greenhouse, but found that fine sediments were fatal to red alder seedlings (Chenoweth et al., 2011). This suggests that sediment or soil moisture is critical for red alder seedling survival. Therefore, an understanding of moisture and evaporation in the system is critical to predicting a possible response of an important native Elwha species such as red alder.

1.4 Barrier Influences on Microclimate and Vegetation

Biotic and abiotic objects that create structure in an environment, such as plants, rocks, buildings and woody debris affect their nearby microclimate (Gray and Spies,

1997; Peters et al., 2008; Bang et al., 2010; Armas et al., 2011). In many instances, and especially where evaporation demand is high, manipulation of microclimate, by causing windbreaks and shade, may be desired to make conditions more favorable for plants (Skidmore and Hagen, 1973; Gray and Spies, 1997). Increasing heterogeneity of microclimate and including more favorable microclimate sites within an area allows plants to establish themselves in disturbed areas (Kupferschmid and Bugmann, 2005; Blood and Titus, 2010; Pastur et al., 2014).

Mayaud et al. (2016) studied the varying effect on leeward wind turbulence of three morphotypes of plants. They found that grass clumps reduced mean wind velocity by 70% and shrubs reduced mean wind velocity by 40%, both in the immediate lee. Both the grass clumps and the shrubs reduced wind velocity for a distance of about nine times their height downwind. The trees measured in this study increased wind speed below their crown to about three tree-heights leeward, but slowed wind speed at the ground surface from three to eight tree-heights downwind. Previously, more general studies on windbreaks have found that wind breaks reduce wind velocity downwind for a distance of two to five times the object's height (Brandle et al., 2006).

Established, living plants can reduce environmental stress for other plants nearby, which is particularly relevant in areas of high environmental stress (Fryrear and Skidmore, 1985; Armas et al., 2011; Supuka and Uhrin, 2016). This effect is particularly important for the success of early plant life stages such as germination and establishment (Peters et al., 2008). However, there are some negative interactions between the plant and its affected partner plant. Live plants deplete soil moisture and nutrients in a localized area (Gray and Spies, 1997). Armas et al. (2011) found that in the most arid environments, plant species could only exist in the proximity of an assisting shrub species, *Retama sphaerocarpa* L. (Boiss). Butterfield et al. (2016) and Maestre et al. (2006) observed variable community response to drought in desert shrub communities, suggesting that some positive plant-plant responses to drought exist between individuals of different species(Armas et al., 2011). Other studies have suggested that positive plant-plant interactions during environmental stress can be observed at

the community level in addition to the individual level (Bertness and Callaway, 1994; Lortie and Callaway, 2006; Maestre et al., 2009; Holmgren and Scheffer, 2010).

Rocks influence microclimate similar to plants in respect to both water availability, and reduced temperature and incident solar radiation (Peters et al., 2008). Peters et al. (2008) determined that water availability is extended 19 days after a rain event when close to rocks, surface temperature can drop as much as 7 ^{o}C between 50 cm and 0.5 cm from a rock, and, dependent on the rock shape and size, rocks can create dense shade. Xeric plant species preferentially develop root systems near rocks and some preferentially grow near rocks (Peters et al., 2008).

Where evaporation is high, windbreaks reduce evaporative stress to plants and reduce mechanical damage to plant tissues (Skidmore and Hagen, 1973). The extent of this effect depends on how much the leeward airflow changes and how that change influences overall microclimate. Windbreaks reduce the leeward horizontal wind speed, alter the leeward vertical air flow and stimulate turbulence. This reduction of horizontal wind is dependent on the speed and incident angle of wind, and also dependent on the permeability and height of the wind barrier (Woodruff et al., 1963; Skidmore and Hagen, 1973; Grace, 1977; Fryrear and Skidmore, 1985; Heisler and Dewalle, 1988; Brandle et al., 2006; Mayaud et al., 2016). The leeward wind break region can extend to a distance 30 times the height of the object breaking the wind (Grace, 1977). Bang et al. (2010) discovered that windbreaks caused by buildings in desert cities increase plant productivity, which in turn has an effect on the abundance and diversity of higher trophic levels in these areas.

1.5 Woody Debris in Plant Establishment

Woody debris creates microsites and alleviates environmental stresses associated with hot, dry summers in the Pacific Northwest (Gray and Spies, 1997). In clear-cuts, stumps have been found to provide better microsites than living vegetation. Because LWD placed on the ground surface creates a barrier to wind, slowing horizontal

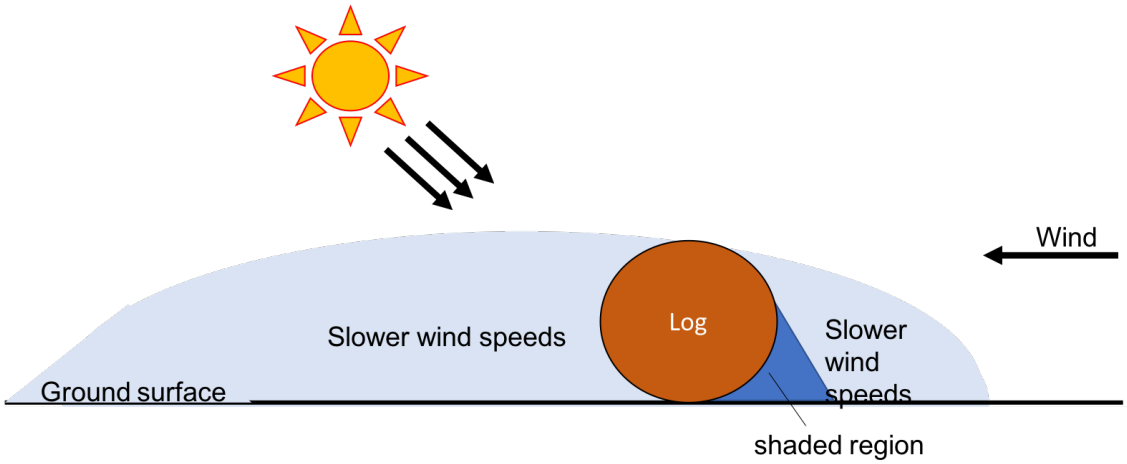

Figure 1.4: Logs may manipulate microclimate by creating an area of shade and regions where horizontal wind speeds are slowed. A larger region of slowed wind speeds exist to the leeward region than to the windward. The slowed horizontal wind speeds in these regions suggest increased turbulence. Shade exists where the log blocks the direct sunlight from reaching the ground surface.

wind at short distances to the windward sides and also to larger distances to the lee (Rosenberg et al., 1983) (Figure 1.4). As wind approaches the windward side of the log, it puts pressure on the log surface and the wind is redirected, causing a small region of slowed wind. To the lee, horizontal wind speeds near the ground are also slowed due to the redirected air flow. The amount of turbulence in these regions may be increased due to the log having low porosity of air flow.

Fine woody debris has been shown to increase natural recruitment and regeneration of *Nothofagus pumilio* in a harvested forest patch, by increasing the proportion of favorable microclimate in logged areas in southern Patagonia (Pastur et al., 2014). Fine woody debris reduced air temperatures and increased soil water content which could be important for establishing vegetation in former Lake Mills. This region in Patagonia is climatically different from the Elwha watershed with different limiting factors. While this Patagonia study site is primarily light-limited for the target species, drained Lake Mills is expected to be moisture-limited (Gray and Spies, 1997; Chenoweth et al., 2011). However, this discovery that woody debris increases the variability of microclimate and increases natural recruitment could also apply to the

Elwha watershed system and others.

LWD is convenient to use as a barrier in a dam-removal scenario because logs have often accumulated around shorelines of previous reservoirs and are readily available (Chenoweth et al., 2011). In Lake Mills, LWD is expected to assist vegetation by not only providing improved microclimates, but also aiding in accumulating organic matter and reducing herbivory (Chenoweth et al., 2011).

1.6 Dewatered Sediments as a Novel Environment

Dam removal science is relatively new and large gaps in literature on the effects of dam removals exist (Bellmore et al., 2017). Only 9% of dam removals in the U.S. have published scientific literature associated with them. Out of these, vegetation studies are relatively rare and primarily focus on riparian vegetation near the river channel and succession near the former shoreline of the reservoir (Auble et al., 2007; Bellmore et al., 2017).

Exposed reservoir sediments create a unique landscape pattern compared to the surrounding areas and therefore can create a unique set of processes, or microclimate, in the environment as compared to the surrounding forest landscape (Turner, 1989). These sediments contain little to no organic matter and do not contain biological legacies. Therefore primary succession is expected to occur similar to succession after glacial retreat or volcanic eruption (Walker and Del Moral, 2003; Chenoweth et al., 2011).

Sediment terraces within Lake Mills and Lake Aldwell are expected to form novel vegetation communities because some plant species may be more tolerant to the unique environmental stresses present in reservoir sediments than others or may be more likely to germinate under the unique environmental conditions (Chenoweth et al., 2011; Schuster, 2015).

Based on previous research in environments other than dewatered sediments, I can predict some aspects of microclimate of dewatered Lake Mills sediments and

limiting factors to plant life there. In desert regions, shortwave and emitted thermal radiation from the ground are relatively high due to light coloring of ground surfaces and high surface temperatures, respectively (Rosenberg et al., 1983). Because of the low moisture and minimal vegetation on Lake Mills sediments, the outgoing radiation properties here may be similar to desert regions, with higher ground temperatures compared to other surface types in the Elwha watershed. As described in Section 1.3.3, Haeussler et al. (1995) observed the combined effects of heat and drought stress on red alder, they suggested that temperature variability and daily maximum temperature may have an effect on distribution of red alder, separate from an effect from soil moisture. Mineral soil exposure, as in this study, presents a similar scenario to Lake Mills sediments and red alder is an important Elwha species (Chenoweth et al., 2011).

Placement of large woody debris is important for the Elwha restoration if the manipulated microclimate around logs allows plants to establish and survive in patches where they would not otherwise survive (Kupferschmid and Bugmann, 2005). Established plants nearby to logs can also manipulate microclimate to recruit even more vegetation (Fryrear and Skidmore, 1985; Armas et al., 2011; Supuka and Uhrin, 2016). As more vegetation establishes, these once bare and inhospitable sediments on the Lake Mills valley-bottom can begin to become more similar to the forests that surround them.

1.7 Study Objectives and Questions

The main objective of this study is to determine how LWD affects microclimate in dewatered Lake Mills, WA during the most moisture-limited season. To achieve this objective, three main questions were assessed:

1) **What is the spatial pattern of microclimate in the vicinity of a log?**

Hypothesis 1a: Microclimate varies with distance and direction from a

log.

Hypothesis 1b: On the shaded, windward (north) side of a log, wind speed, sediment temperature and evaporation rate will decrease near the shaded, windward (north) side of a log.

Hypothesis 1c: On the sun-exposed, leeward side (south) of a log, sediment temperature increases or remain the same, and wind speed and evaporation rate decrease with proximity to the log.

2) **What is the temporal pattern of microclimate in the vicinity of a log?**

Hypothesis 2: The spatial pattern of microclimate remains the same within a day and among days, but the ranges of the values of microclimate vary within a day and among days.

3) **How are the spatial and temporal patterns of microclimate quantitatively related to broader environmental factors?**

Hypothesis 3a: Wind speed at 10 cm height is a function of wind speed at greater heights and recent solar radiation.

Hypothesis 3b: Sediment temperature is a function of recent solar radiation and air temperature.

Hypothesis 3c: Evaporation rate is a function of recent solar radiation, air temperature, vapor pressure deficit and wind speed at 1 m height.

Chapter 2

Methods

2.1 Site Description

The Elwha River watershed encompasses approximately 860 km^2 and is located on the Olympic Peninsula, WA (Chenoweth et al., 2011). The Elwha flows from the Olympic Mountains north to the Strait of Juan de Fuca. A majority of the Elwha watershed (83 %) is inside the Olympic National Park Boundary (Chenoweth et al., 2011; Randle et al., 2015). The 99-year old Elwha Dam which once impounded Lake Aldwell at river km 4.9 was removed in 2011 and the Glines Canyon Dam, which once impounded Lake Mills for 87 years at river km 21.6 was fully removed as of September 2014. The Lake Mills site now contains approximately 1.77 km^2 of newly exposed land surface (Chenoweth et al., 2011) (Figure 2.1). An estimated 16.1 million cubic meters of sediment were left behind on the Lake Mills valley bottom (Randle et al., 2015). Approximately half of the sediments are fine (silt and clay) and half are course (sand, gravel and cobbles) (Chenoweth et al., 2011).

Revegetation of these sediments is a goal of the Elwha restoration plan with the objectives to minimize invasive species, restore ecosystem processes and establish native forests within the dam removal areas (Chenoweth et al., 2011). Harsh, unsuitable environments and greater distances from established vegetation around the former shoreline are expected to be challenges to revegetation of Lake Mills sediments.

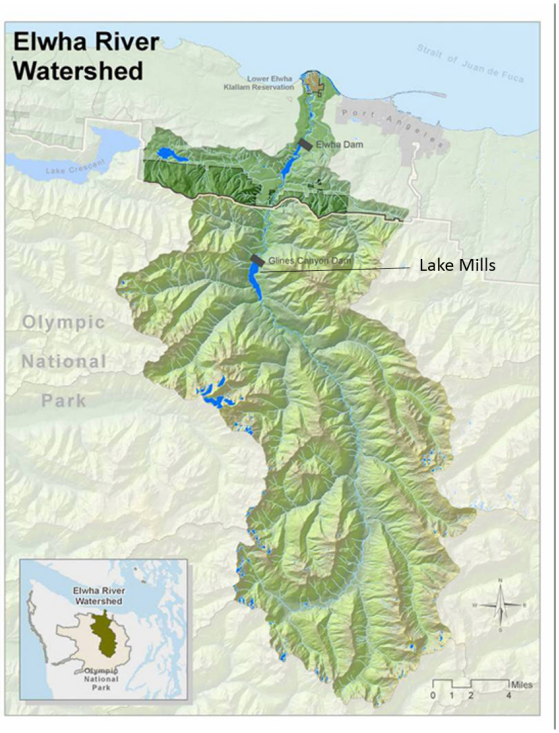

Figure 2.1: Elwha River watershed on the Olympic Peninsula in Washington, USA. Former Lake Mills is located at river km 21.6, within the boundary of Olympic National Park. Image courtesy of the National Park Service.

On October 2, 2014, Olympic National Park placed 395 pieces of LWD on the exposed Lake Mills lake-bottom sediments over a 2.6 km^2 area by helicopter to aid in revegetation efforts by providing areas of more suitable microclimate (Chenoweth et al., 2011; McHenry and Chenoweth, 2015). The site of this log relocation is on a raised terrace on the west side of the current, post-dam river channel and is approximately 1 km south of the former Glines Canyon Dam site.

The Elwha River watershed has the steepest precipitation gradient on the Olympic Peninsula, with the upper watershed receiving 550 cm of precipitation annually and the lower watershed receiving 100 cm (Phillips and Donaldson, 1972). During field measurements, from August 20, 2015 through September 7, 2015, weather was variable. Between August 20 and August 27, the local weather was warm, with an average daily temperature between 14.6 ^oC and 18.6 ^oC, and dry with an average relative humidity of between 33.7 % and 42.2 % (Baccus, Personal Communication). There was no rainfall during this period (Baccus, Personal Communication). Between August 28 and September 3, sampling was suspended due to rain (Figure 2.2) (Baccus, Personal

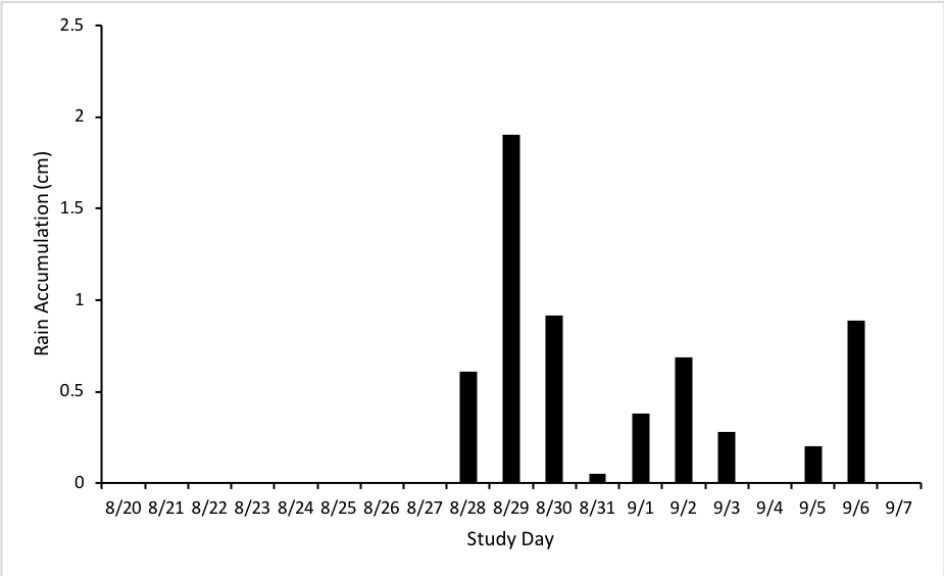

Figure 2.2: Rainfall accumulation was recorded at the Elwha Ranger station to the north of Lake Mills. Data for this study were not collected on days when rain was falling, except 9/5, but it was not raining in former Lake Mills while measurements were taken. Rainfall accumulation data were collected by Olympic National Park (Baccus, Personal Communication).

Communication). During this time, the average daily temperature was between 10.4 ^{o}C and 16.1 ^{o}C. A total of 4.83 cm of rain fell during this period, averaging 0.69 cm per day. Relative humidity was not recorded for this time period. Between September 3 and September 7, the average temperature was between 10.3 ^{o}C and 13.0 ^{o}C and the relative humidity was between 53.3 % and 83.6 %. A total of 1.1 cm of rain fell during this period, but rain was not falling during transect measurements (Baccus, Personal Communication).

2.2 Sampling Design

The log on the north end of the LWD relocation site, called "repeated", was selected for repeated measurement on 10 days and measurements were taken multiple times on an additional day (Figure 2.3). Eight more logs, called "other logs", were randomly selected for microclimate measurement within the October 2014 log drop site. For the random selection, a grid containing 18.7 by 18.7 meter squares was overlaid on an aerial image of the study site. Points on this grid were randomly selected using a ran-

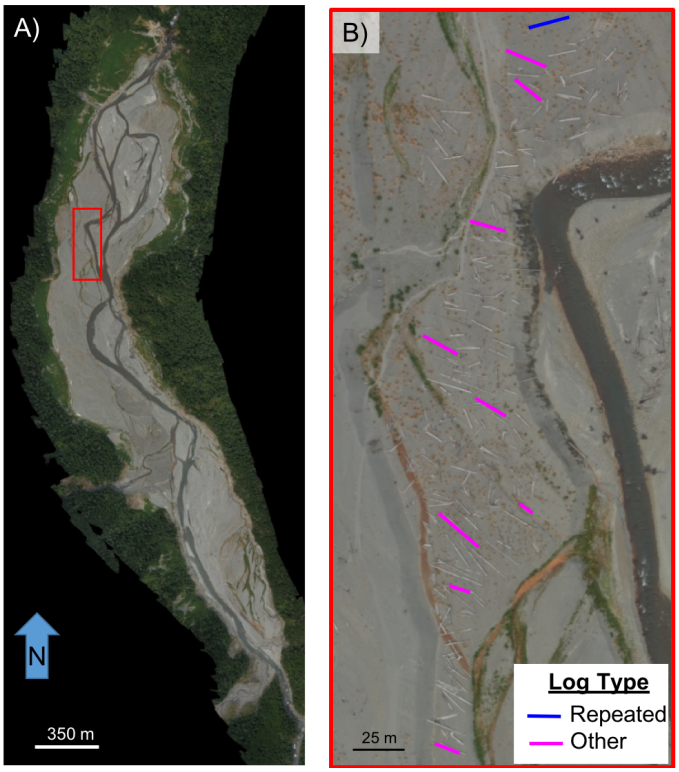

Figure 2.3: October 2014 LWD relocation area within Lake Mills. A) shows the October 2014 LWD relocation area within former Lake Mills, highlighted with a red rectangle. B) is an enlarged image of the LWD relocation site highlighted in A). Logs highlighted in magenta and blue are logs sampled for this study. Blue is the repeated log, magenta are others logs. Aerial imagery courtesy of Andy Ritchie (USGS).

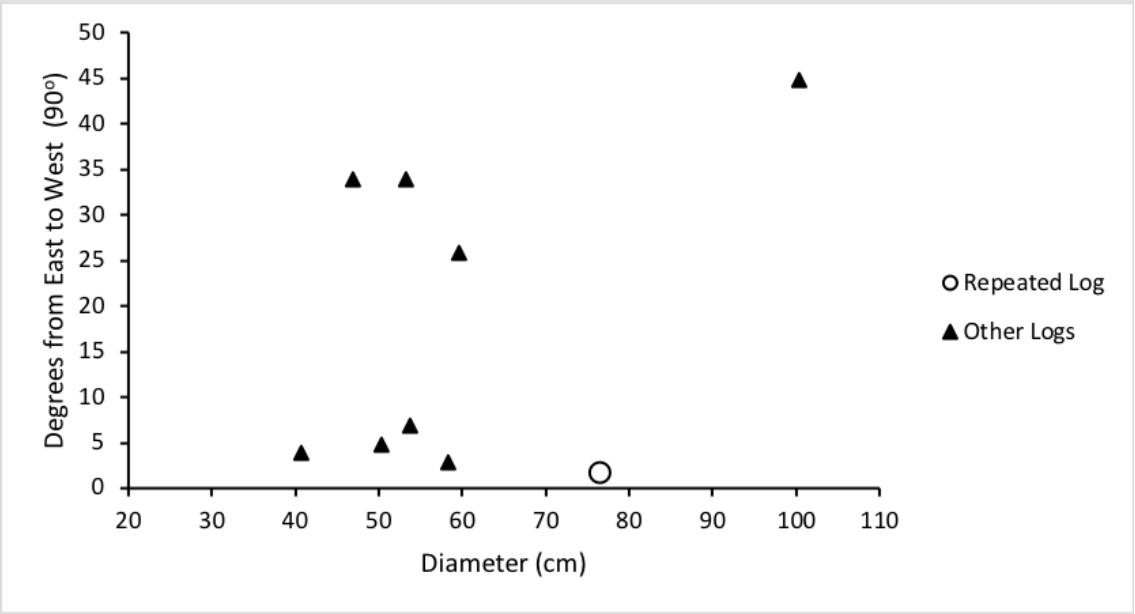

Figure 2.4: Logs sampled for this investigation had a range of diameters between 40 cm and 100 cm, and varied orientation deviation from east-west (90^o) between 2^o and 45^o. Deviation from east-west is the absolute value of the log's orientation - 90^o.

dom number generator (Random Number Generator application for iOS, Alexander Rutkowskij). The nearest log to this coordinate point that fit the log criteria (Section 2.3) was selected for measurement. Other logs were transected only once each, on the same days that the repeated log transect measurements were taken.

2.3 Log Criteria

Logs selected for this study met criteria of location, size, orientation and decay class to be comparable to one another, while the sample was still random enough to adequately provide information about the population of logs within the October 2014 LWD relocation site. Criteria for selected 'other' logs included: location greater than 5 m from the eastern or western terrace edge, diameter between 30 cm and 100 cm, log touches the sediment surface for over one third of their length, greater than 3 m from another log, and oriented within 45 degrees of East-West. An additional criterion was that selected logs must also be in the decay class 3 (no bark present, but remains intact when kicked) on a five point decay classification system adapted from Palace et al. (2007) and Larjavaara and Muller-Landau (2010). Selected logs

represented a diversity of diameters and orientations of LWD found in the October 2014 LWD relocation site (Figure 2.4). I was unable to identify the species of the logs, but the criteria for chosen logs helps ensure that all selected logs may act similarly on microclimate.

The average diameter of the log was calculated from three diameter measurements: one at one third the total length of the log, one at two thirds the total length and one at the transected point of the log. The transected point of the log is the point on the log which was transected for microclimate variables (See Section 2.4) Diameters were measured horizontally using a rod with two plumb bobs attached. The orientation of the log was measured with a compass aligned along the length of the log.

The two nearest logs within 10 meters of the transected point on the measured log were recorded. If no logs existed within 10 meters, only one nearest log was measured. Distance and orientation to nearest logs were measured from the transected point on the measured log to the nearest point of the nearest log using a meter tape and compass, respectively.

2.4 Transect Design

Microclimate measurements were taken along a north and a south transect extending perpendicularly from each selected log. Each transect began at the point at which the log touches the sediment (0 cm) and extended 300 cm away from the log (Figure 2.5). Transects of logs were located within the middle third of the log length and were located where the log was touching the sediment surface and there were the least amount of obstacles (vegetation and large rocks) that would hinder microclimate measurement 300 cm in either direction from the log.

Sediment temperature and evaporation rate were measured at 5, 10, 15, 30, 45, 60, 75, 90, 120, 180, and 240 cm to the North of the log, and 5, 10, 15, 30, 45, 60, 75, 90, 105, 120, 135, 150, 180, 210, 240 and 270 cm to the south of the log on August 20, 2015 only. On all other sampling days, sediment temperature and evaporation

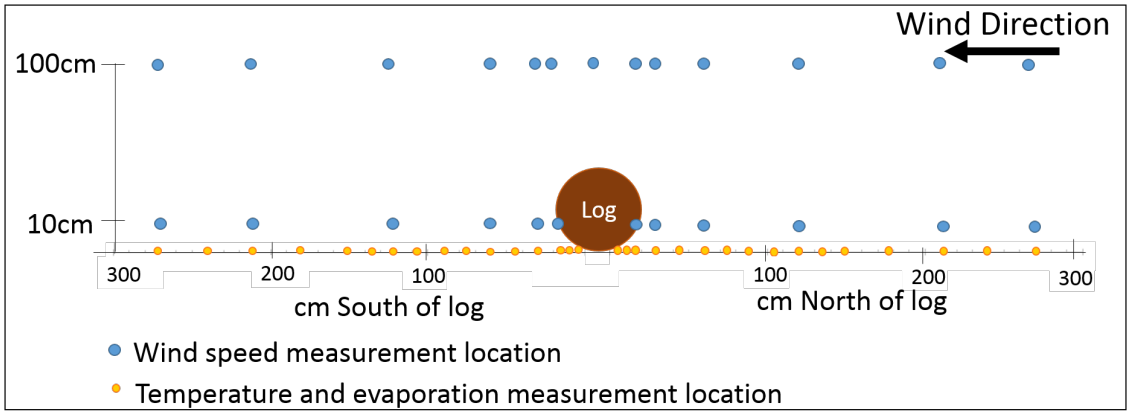

Figure 2.5: Microclimate measurement locations along log transect. Side view (from the East, looking West) of a transected log, with locations of sediment temperature and evaporation measurements (yellow dots) and wind speed measurements at 10 and 100 cm (blue dots). During all transect measurements, the wind direction was approximately North

rate were measured at the same distances, but also included measurements at 105, 135, 150, 210 and 270 cm to both the north and south of each log. Wind speed was measured at 10 cm and 100 cm above the sediment surface at distances of 10, 20, 30, 60, 120, 200 and 300 cm on both the north and south sides of each log on August 20, 2015 only. For all other sampling days, wind speed at 10 and 100 cm were measured at 10, 15, 30, 60, 120, 210 and 270 cm to the north and south of each log (Figure 2.5). Due to the shape of some logs measured, it was not possible to place equipment at transect points closest to the log. In these instances, measurement at these points were not taken.

2.5 Microclimate Measurements

Microclimate measurements of sediment temperature, wind speed and evaporation rate were measured on a transect of the repeated log five times on August 21, 2015 and 10 times between August 20 and September 7, 2015 to assess spatial patterns of microclimate near a log and how they vary temporally (Table 2.1). Selected other logs were measured during the same period, but at different times as the repeat log among-day measurements except August 21, 2015.

Table 2.1: Times of transect measurement of the repeated log. The repeated log was transected 14 times in 10 days between August 20, 2015 and September 7, 2015. All times are in standard time.

Study Day	Date	Time
1	8/20	14:45
2	8/21	9:28
2	8/21	11:30
2	8/21	13:33
2	8/21	15:20
2	8/21	17:06
4	8/23	14:09
5	8/24	12:09
6	8/25	14:28
7	8/26	12:40
8	8/27	12:30
16	9/4	8:35
17	9/5	14:36
19	9/7	12:24

2.5.1 Wind Measurement

Average wind speed (u) perpendicular to the log was measured using anemometers (Kestrel 3000, Forestry Suppliers, Inc., Jackson, MS) over a 30 second period. Two anemometers were attached to a meter stick at 10 cm and 100 cm heights from the sediment surface and averages at both heights were recorded simultaneously. Transects were repeated twice and the two 10-cm height wind speeds (u_{10}) recorded at each transect distance and height were then averaged to create the u_{10} data used for analysis. All 100-cm height wind speed ($\bar{u}_{100}$) measurements were averaged to create a single value for the entire transect. Averages were used to reduce the noise in u data caused by momentary gusts.

2.5.2 Sediment Temperature Measurement

Sediment temperature (T_S) was measured using shaded digital thermometers (Traceable ® Lollipop ™ Waterproof/Shockproof Thermometer, Control Company, Friendswood, TX) at 3 cm depth along the transect. Measurements were taken as close to the tran-

sect line as possible, but if the sediment inhibited the insertion of the thermometer due to the presence of a rock, it was moved to the nearest possible location at the same distance perpendicular to the log. Thermometers were allowed to equilibrate for approximately one minute before temperatures were recorded.

2.5.3 Evaporation Measurement

Evaporation rate (E) (mg of water loss per minute) (mg/min) was measured gravimetrically using moistened tennis balls (Wilson ® EXTRA DUTY, Wilson Sporting Goods Co., Chicago, IL). In containers containing three tennis balls each, balls were submerged in tap water for at least one minute, then dried to a mass of 71±1 grams using hand towels. The water was discarded and the tennis balls were then allowed to equilibrate in the same container for at least 30 minutes. Each tennis ball was weighed just prior to deployment, then was placed on a 1-inch high plastic ring at the desired transect point. After 40±1 minutes or 30±1 minutes each ball was reweighed. The evaporation rate in mg/min was calculated from the difference between the initial mass and mass after elapsed time, divided by the total elapsed time. All weights were ± 0.1 g accuracy and quality control measurements were taken with a 200.0 g weight periodically during measurement. An ancillary study indicated that the 10 minute difference in exposure time does not influence E (Appendix A).

2.5.4 Weather Data

Before each transect was measured for the aforementioned microclimate variables, the air temperature at 1 m height (T_a) was recorded from two digital thermometers at the log where the transect bisects the log (Traceable ® Lollipop ™ Waterproof/Shockproof Thermometer) and the relative humidity (%) of the air was recorded from two combined anemometer/hygrometers (Kestrel 3000) and averaged. Relative humidity was precise to ±2%. The vapor pressure deficit (ρ) was calculated from average T_a and relative humidity for each transect measurement using the equation $\rho = SVP\frac{100-RH}{100}$ (Monteith and Unsworth, 1990). In this equation, SVP is the satu-

rated vapor pressure of water in the air at the measured air temperature. The SVP is calculated from an adapted version of the Tetens equation found in Monteith and Unsworth (2007): $SVP = 0.6108e^{\frac{17.27T_a}{T_a+237.3}}$. The wind direction was estimated by noting the direction for which the maximum u was recorded on the combined anemometer/hygrometer (Kestrel 3000). Presence of shade on the sediment was recorded for each transect point measured.

A pyranometer (LiCOR 200S, LI-COR ®, Lincoln, NE) at Lake Crescent Laboratory on the north shore of Lake Crescent collected solar radiation data every 5 minutes and provided hourly averages of R_S in Wm^{-2} (Baccus, Personal Communication). Two-hour ($R_{S,2h}$) and four-hour cumulative solar radiation inputs ($R_{S,4h}$) (Whm^{-2}) were calculated from these data for the time periods leading up to the transect measurement start time.

2.6 Statistical Methods

2.6.1 Curvilinear Transect Model Selection

Curvilinear regression models of microclimate variable versus distance from log were used to make qualitative observations of spatial and temporal microclimate patterns around logs.

Curvilinear regression analysis was completed using SPSS for each microclimate variable, to the north and south (IBM SPSS Statistics version 24.0, IBM, Armonk, NY) for each transect of the repeat log. Transects were fit with linear, logarithmic, quadratic, compound, power, S, growth, exponential and logistic curves. SPSS generated the optimal equation for each curve type, an ANOVA analysis of the curve, and another ANOVA of the significance (P value) for each of the coefficients. Out of the acceptable curves for each transect ($\alpha = 0.050$ for all described ANOVA results), the curve that created all physically possible results and with an R^2 within 0.100 of the maximum generated R^2 was chosen to represent that transect. The limits on physically possible results between 0 and 300 cm distances were 0 to 4.2 m/s for u_{10},

0 to 40 ^{o}C for T_S and 0 to 150 mg/min for E. These curves only describe the transect between 0 and 300 cm, because data were not taken outside of this range. If there were no acceptable curves for a transect, the average value was used to represent all distances (y = average of all values). The assumptions of curvilinear regression were not evaluated in this analysis.

2.6.2 Multilevel General Model Selection

A multilevel modeling technique (Heck et al., 2013) was used to determine quantitative relationships of microclimate variables to distance from log and weather variables. This approach was required because points within a transect are not independent from one another.

Instead, individual transects were considered clusters of measured transect points, where:

$$\text{For each transect } j\text{, microclimate variable value at point } i = f(distance_i)$$

This represents the first level of regression in this analysis and was created by regressing each transect measured with a common function (see Section 2.6.2.1).

These regression equations resulted in model function parameters ($maxV$, maxeffect, dhalfmax or average value (Section 2.6.2.2)) that represent each transect j, which were then regressed with environmental factors including local weather variables. This is the second level of the multilevel model.

$$\text{model parameter} = f(\text{environmental factors}_j)$$

When the regressions from the second level are substituted back into the first level, the result is a model that includes explanatory variables from both levels to predict the value of a specified microclimate variable at any point of a given log transect with known distance from the log and environmental factor information:

$$\text{microclimate variable value at point } i \text{ within transect } j = f(\text{distance}_i, \text{environmental factors}_j)$$

2.6.2.1 Common Functions

For north and south u_{10}, north T_S, and north E versus distance from log, I fit a two-line segment model to represent the data. This model is represented by the general equation:

$$value = minimum(a + bd, maxV)$$

Where a and b are the intercept and slope of a line segment, d is the distance from the edge of the log and $maxV$ is a line with a slope of 0 representing another line segment. The minimum of these two line segment values creates a model where there is a sloped line at distances closer to the log, but then reaches a maximum value ($maxV$) for distances farther from the log (Figure 2.6). Model parameters a, b and $maxV$ were estimated using SPSS nonlinear regression analysis and adjusted R^2 values are reported.

Each two-line segment model was reformulated into the following form:

$$value = minimum((maxV - maxeffect) + \frac{maxeffect(d)}{2(dhalfmax)}, maxV)$$

with three common model parameters: maximum value (maxV), maximum effect (maxeffect) and the distance to half maximum effect (dhalfmax). The maxV is derived from the nonlinear regression output and is the maximum value of the parameter, experienced at greater distances from the log. The maxeffect is the maximum increase or decrease in the microclimate variable's value experienced closer to the edge of the log. This parameter is calculated by

$$\text{maxeffect} = \text{maxV} - a.$$

The dhalfmax is the distance from the log at which half of the maximum effect of the log is experienced. dhalfmax is calculated by

$$\text{dhalfmax} = \frac{0.5(maxeffect)}{b}.$$

South T_S and south E transects did not visually fit this pattern and were both represented by the average value at all distances.

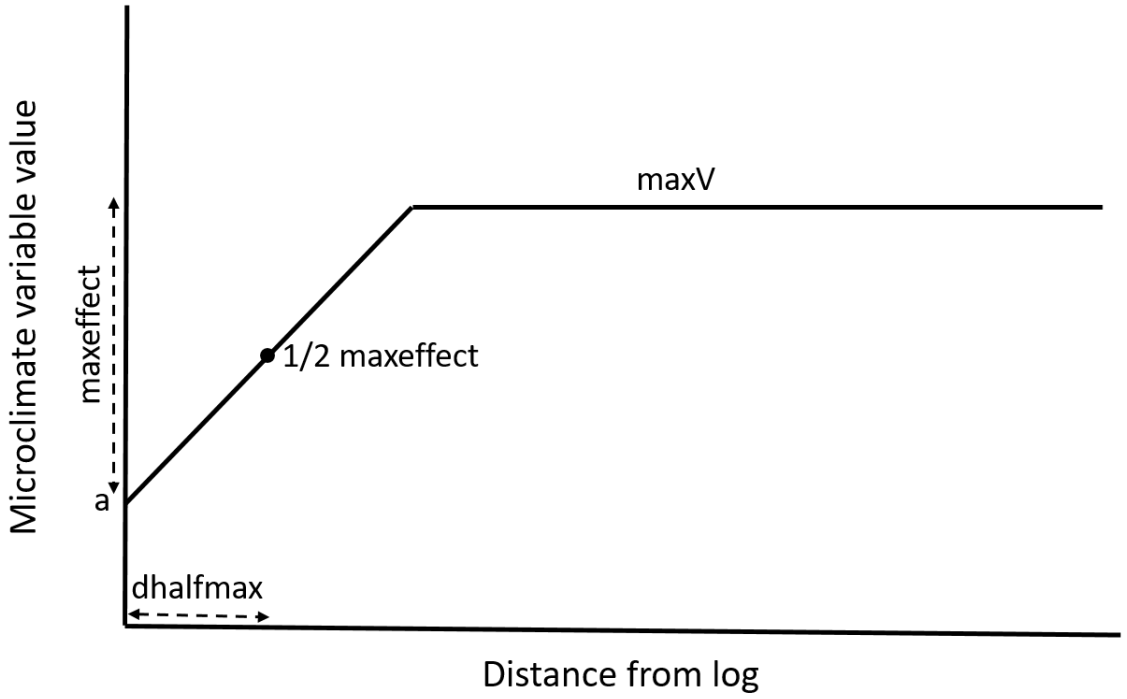

Figure 2.6: The two line segment model used as the common model for north and south u_{10}, north T_S and north E, with coefficient-derived variables of maxV, maxeffect and dhalfmax shown graphically. This model is mathematically presented as: $value = minimum((maxV - maxeffect) + \frac{maxeffect(d)}{2(dhalfmax)}, maxV)$. This model (f(distance)) represents the first level of the multilevel regression.

2.6.2.2 General Models

Common model parameters $maxV$, maxeffect and dhalfmax were then individually regressed against relevant weather variables in SPSS using curvilinear analysis, and linear analysis (with one or more independent environmental factors). The independent environmental factors attempted in these regressions were chosen based on known conceptual relationships described in Section 1.2. For transects of u_{10}, independent variables chosen were $\bar{u}_{100}$, $R_{S,2h}$ and $R_{S,4h}$. For transect of T_S, independent variables chosen were average T_a, $R_{S,2h}$, $R_{S,4h}$, and R_S. For transects of E, independent variables chosen were ρ, $\bar{u}_{100}$, and R_S.

For the south T_S and south E transects, the average value itself was regressed against relevant weather variables in SPSS and these regression equations were used to predict the value of T_S and E to the south of the log.

The best combinations of parameter regressions were chosen by how well they fit the repeated log data. Models that maximized adjusted R^2 values between measured and modeled values of u_{10}, T_S, and E, and whose linear regressions' slope and intercept were closer to 1 and 0, respectively were most ideal. If two or more models fit similarly, the simplest model with fewer input variables was preferred.

2.6.2.3 General Model Validation

The general model was used to predict values of microclimate variables for the eight randomly-selected other logs to assess how well the models may apply to other logs with varying location, size and orientation within the October 2014 log drop area. Slopes of linear regression fits of modeled versus measured data points for model-informing, repeated log transects were compared to the slopes of linear regression fits of modeled versus measured data for the other-log, validation transects using t tests. Significant differences in slopes of other-log (validation data) fit and repeated-log (model-informing) fit support differences in the factors creating microclimate patterns nearby the repeated-log and other logs.

2.6.2.4 Influence of Units of Distance

To test if log diameters are a more appropriate unit of distance than centimeters in these models, all distances were converted to units in log diameters, specific to the log measured, using the average log diameter measurement.

$$distance(diameters) = \frac{distance\ (cm)}{average\ log\ diameter\ (cm)}$$

Logs were assumed to be approximately round and diameters measured horizontally are assumed to equal the height of the log from the sediment surface. I predicted that expressing distance units in diameter would improve model fits because effects of windbreaks are directly related to the height of the windbreaking object, and these units are typically used in windbreak studies (Grace, 1977; Fryrear and Skidmore, 1985; David et al., 2016; Mayaud et al., 2016). The height of the log also affects the distance that shade extends from the log, which may influence sediment temperature and evaporation rate.

Chapter 3

Results and Discussion

3.1 Weather Patterns

Weather variables recorded for each repeated log transect show some visible similar trends, reinforcing concepts in the conceptual models of microclimate (Rosenberg et al., 1983; Geiger et al., 2009) (Figures 3.1 and 3.2). Greater air temperature (T_a), average wind speed at 1 m height ($\bar{u}_{100}$) and vapor pressure deficit (ρ) all often occur together and with decreased relative humidity.

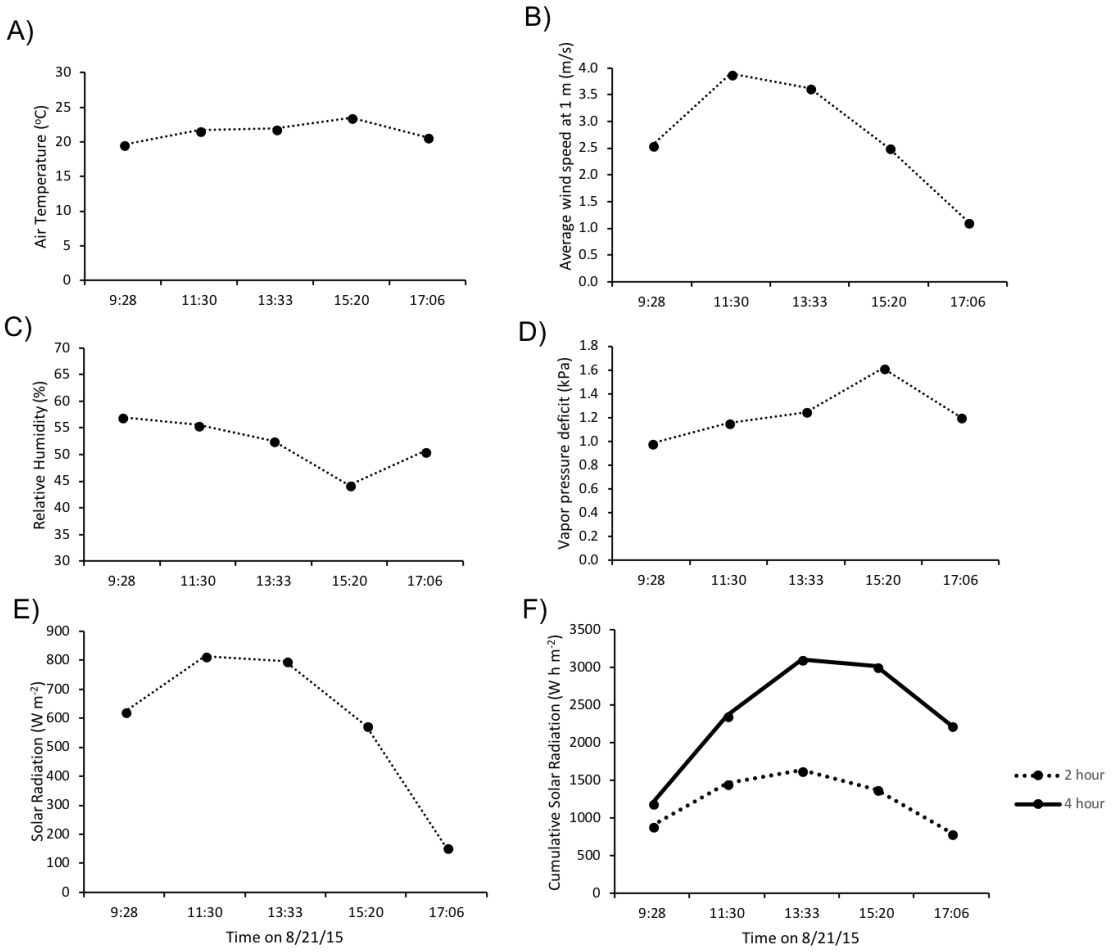

Figure 3.1: Local weather from on-ground measurements and nearby weather stations on August 21, 2015 with times in PST. Variables include air temperature (T_a, ^{o}C) (A), average wind speed at 1 m height($\bar{u}_{100}$, m/s) (B), relative humidity (%) (C), vapor pressure deficit (ρ, kPa) (D), solar radiation (R_S, W m^{-2}) (E) and two-hour and four-hour cumulative solar radiation ($R_{S,2h}$ and $R_{S,4h}$, Whm^{-2}) (F). T_a, relative humidity and $\bar{u}_{100}$ were all recorded at the repeated log at the time of measurement. The R_S was collected by Olympic National Park at the Lake Crescent weather station. There was no rainfall accumulation recorded during this period. Solar radiation measurements in E) were recorded every 5 minutes, and average hourly values of these are reported in W m^{-2}. The $R_{S,2h}$ and $R_{S,4h}$ in F) was derived from R_S data presented in (E) for 2 and 4 hour periods prior to transect measurement.

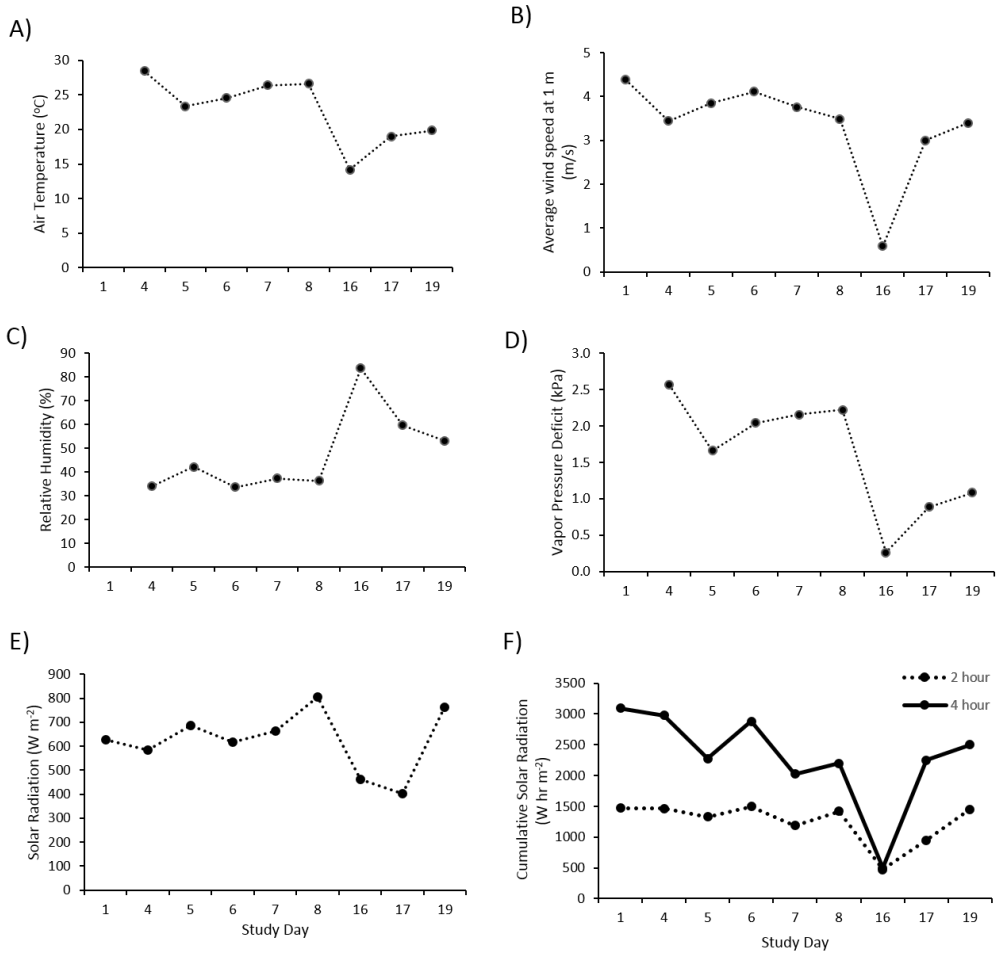

Figure 3.2: Local weather from on-ground measurements and nearby weather stations over the entire study period. Measurements were taken at different times on each study day and are not standardized to a specific time. Each data point corresponds to the time at which the repeated log transect was measured on that day. Weather variables include T_a (^{o}C) (A),$\bar{u}_{100}$ (B), relative humidity (%) (C), ρ (D), R_S (W m$^-$2) (E) and $R_{S,2h}$ and $R_{S,4h}$ (Wh m$^-$2) (F). T_a, relative humidity and $\bar{u}_{100}$ were all recorded at the repeated log at the time of measurement. R_S was collected by Olympic National Park at the Lake Crescent weather station. There was no rainfall accumulation recorded during this period. Solar radiation measurements in E) were recorded every 5 minutes, and average hourly values of these are reported in W m$^-$2. The $R_{S,2h}$ and $R_{S,4h}$ in F) was derived from R_S data presented in E) for 2 and 4 hour periods prior to transect measurement. Measurements were taken at different times on each study day and are not standardized to a specific time. See table 2.1 for relation of study day to date.

3.2 Microclimate Near a Log - Qualitative Evaluation

3.2.1 Curvilinear Models

The curvilinear models outlined in this discussion describe the spatial patterns in microclimate variables at varying distances to the north and south of a repeatedly measured log (objective 1) and are used to qualitatively investigate how these patterns change temporally within a day and among days in the study period (objective 2). Curvilinear regressions to transect data may provide more qualitative detail on these microclimate patterns than a common model, but are not as easily compared quantitatively.

3.2.1.1 Wind Speed at 10 cm Height

Overall, the log influenced u_{10} in two ways. First, u_{10} was slower near the log than farther away on both sides. Between 100 cm and 5 cm from the log, u_{10} decreased 70.7% to the north and 55.8% to the south. Second, u_{10} was, on average, 51.7% slower on the south side than the north side based on maximum values modeled to each side for each transect (study day 16 excluded).

Within-day variability To the northern, windward side of the log, u_{10} sometimes showed evidence of a log-effect, with decreased speeds near the log, for all times measured except 9:28, which showed no pattern (Figure 3.3 A, C). All other times modeled a decrease to under 0.5 m/s within 15 cm of the log. Times differ in the distance north that u_{10} reaches maximum speed. Therefore the estimated distance of the log's effect on u_{10} to the north is variable.

There does not appear to be a consistent effect of the log on u_{10} to the south within 300 cm (Figure 3.3 B, D). However, the decrease in u_{10} from the north to the south, is likely because the log is protecting the leeward side. The u_{10} was more variable to the north than the south of the log. At all times, u_{10} likely causes little stress

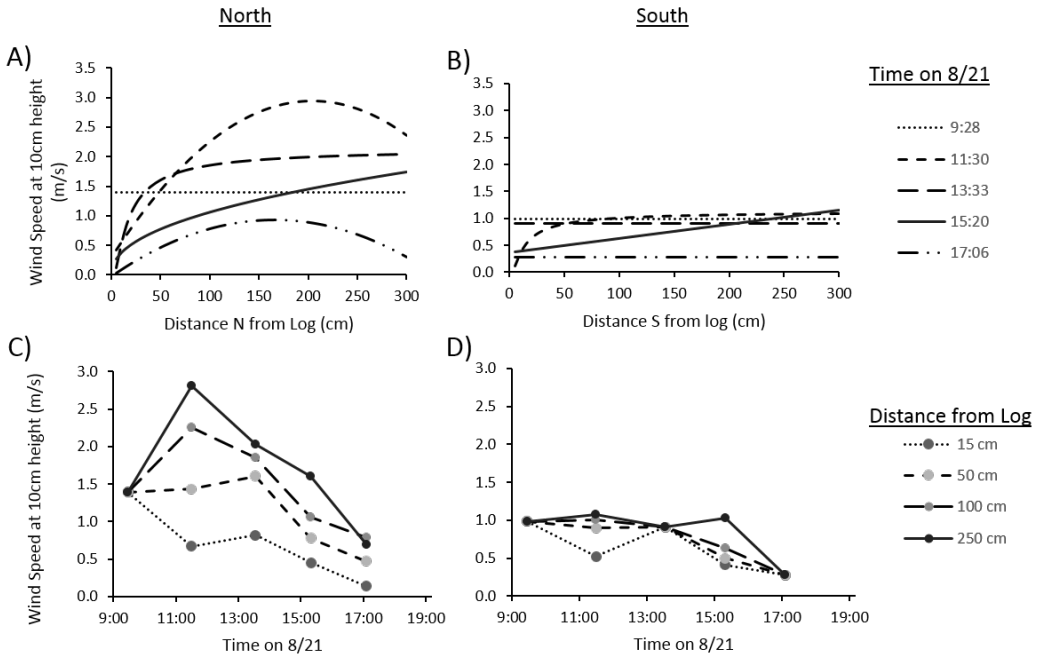

Figure 3.3: Selected curves to represent u_{10} transects for 5 measured times of day on August 21, 2015. Graphs A and C show transects measured to the north of the repeated log and graphs B and D show transects measured to the south of the repeated log. Both graphs A and B both contain a single line generated for that transect at 9:28, 11:30, 13:33, 15:20 and 17:06 measured times. Graphs C and D show modeled u_{10} at four distances of 15 cm, 50 cm, 100 cm and 250 cm from the log repeated five times on August 21, 2015.

to vegetation south of the log, while u_{10} greater than approximately 50 cm north at 11:30 and 13:33 are potentially high enough to affect plant growth (Wadsworth, 1959; Grace, 1977). The slowest u_{10} occurred at 17:06, when the $\bar{u}_{100}$ was also slowest (Figure 3.1).

Variability among days To the north of the log, the u_{10} was lower near the log than farther away except for day 16 when u_{10} was minimal at all distances (Figure 3.4 A). The u_{10} was also slowed to the immediate south of logs for all but one day (Figure 3.4 B). To this direction, however, the difference in u_{10} for the last three days measured was less obvious because u_{10} values appeared to be constrained to less than the range of u_{10} observed to the north.

For all but one day, the u_{10} was lower to the south of the log compared to the north (Figure 3.4). This pattern is consistent with the patterns on August 21, 2015 and is additional evidence that the log slows the horizontal u_{10} on the leeward side.

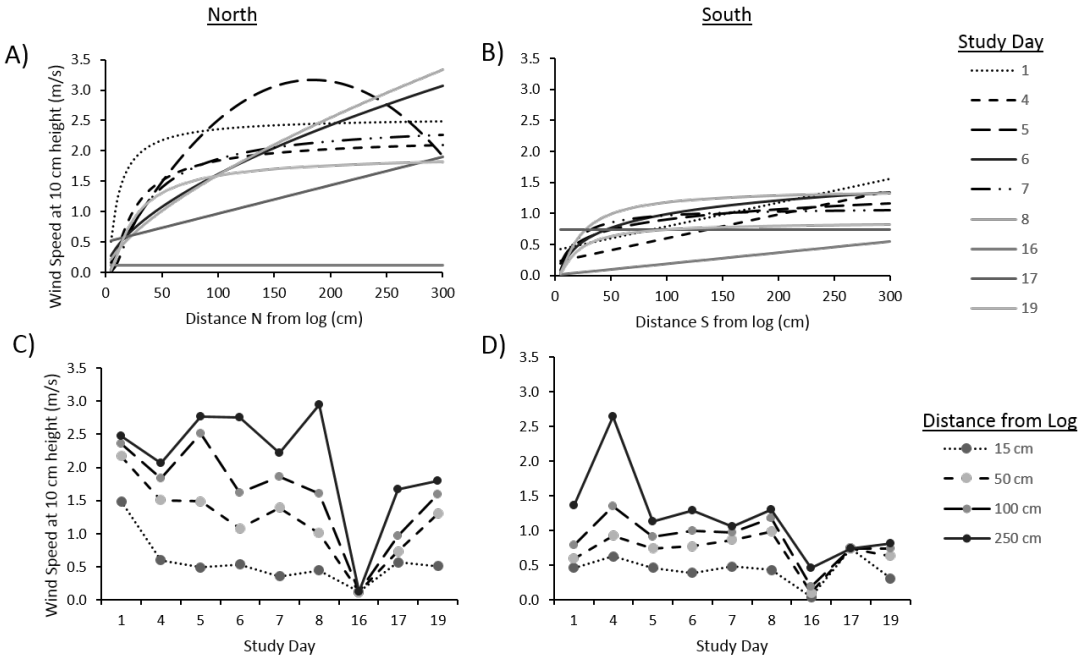

Figure 3.4: The u_{10} (m/s) measured along transects of the repeated log each study day. Graphs A and C show transects measured to the north of the repeated log and graphs B and D show transects measured to the south of the repeated log. Graphs C and D show u_{10} measured at four distances of 15 cm, 50 cm, 100 cm and 250 cm from the log repeated for each study day measured. See table 2.1 for relation of study day to date.

3.2.1.2 Sediment Temperature

Overall, T_S was less near the log than farther away on the north side, but equal or slightly greater on the south side. The T_S far from the log was similar on the north and south sides.

Within-day variability Within 20 cm of the north (shaded) side of the log, T_S was less than that at greater distances (Figure 3.5). This decrease was between 5 and 15 ^{o}C for all times of day except 17:06 which was between 2.5 ^{o}C and 9.3 ^{o}C less. This was probably because the transect was completely shaded during the 17:06 measurements and the sediment was beginning to cool without the solar radiation input. In a desert study site, Peters et al. (2008) reported that surface temperature can drop as much as 7 ^{o}C from 0.5 cm to 50 cm from a rock, which is similar to the pattern observed in Lake Mills. These drops in T_S to the north are likely due to shade cast by the log at that time.

The north transect at 9:28 does not show this drop, but shows a linear relationship with increasing T_S as distance from the log increases. This was the earliest transect measured and therefore did not accumulate as much solar radiation by the measurement time as the other transect times. This pattern in temperature is likely due to a lag in increase of sensible heat within the sediment. Because measurements were taken at a 3 cm depth, the heat must be conducted through the sediment from the surface in order to measure the sensible heat (temperature) at this depth.

Increased T_S occasionally occurred within 20 cm south from the log at 13:33, 15:20 and 17:06, where within 20 cm north, T_S was always decreased (Figure 3.5). Between 20 cm and 300 cm, T_S trends to the south and north had a similar pattern and similar values. Southern T_S remained between 27.3 ^{o}C and 39.0 ^{o}C for all distances and all times (Figure 3.5 B and D).

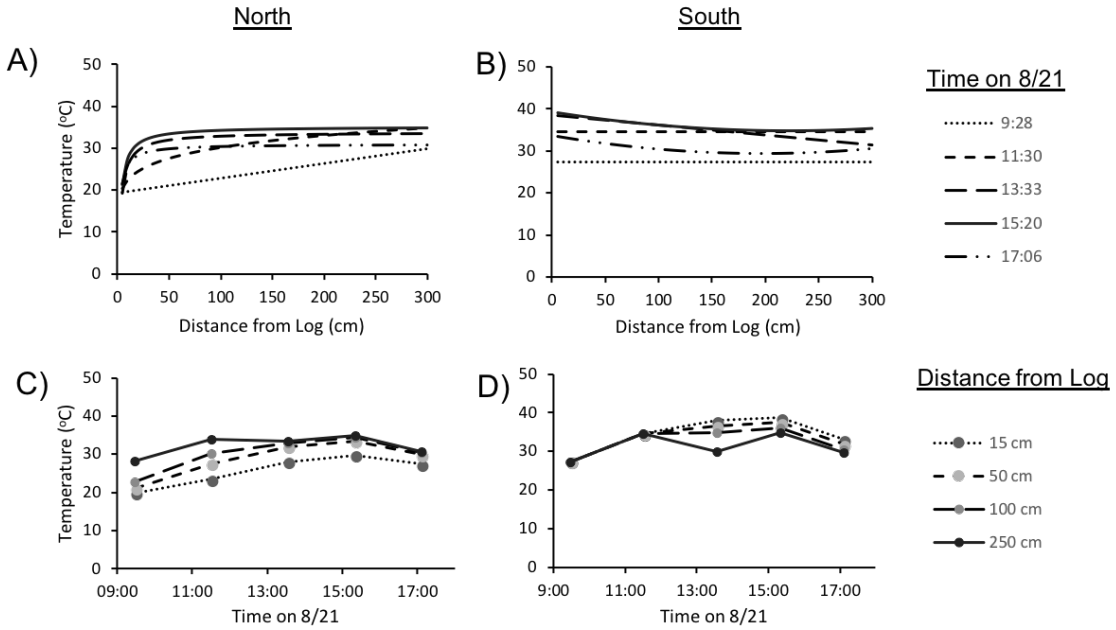

Figure 3.5: Selected curves to represent T_S transects for 5 measured times of day on August 21, 2015. Graphs A and C represent transects measured to the north of the repeated log and graphs B and D represent transects measured to the south of the repeated log. Graphs A and B both contain a single line generated for that transect at 19:28, 11:30, 13:33, 15:20 and 17:06 measured times. Graphs C and D show T_S measured at four distances of 15 cm, 50 cm, 100 cm and 250 cm from the log repeated five times on August 21, 2015.

Variability among days Within 50 cm from the north edge of the log, T_S decreased for all days measured, suggesting that the log creates a consistent effect on T_S to the north (Figure 3.6). However, the magnitude of this effect is variable.

There is some variability in T_S within 25 cm south from the log. A possible log effect to the south of the log on T_S would be relatively small (less than 5 ^{o}C) and could be either an increase or a decrease. On study days 4 and 19, curvilinear models show a slight increase in T_S within 25 cm of the south edge of the log, but study day 7 and 16 models describe a slight decrease in T_S within 25 cm from the south edge of the log.

To both the north and south, T_S values were lowest on study days 16, 17 and 19, which were measured after a rain event. The T_S does not vary much by distance or among days.

The T_S values to the south were between 30 ^{o}C and 40 ^{o}C for all dates and distances, except the days after the rain event: 16, 17 and 19, which were between 10 ^{o}C and 30 ^{o}C.

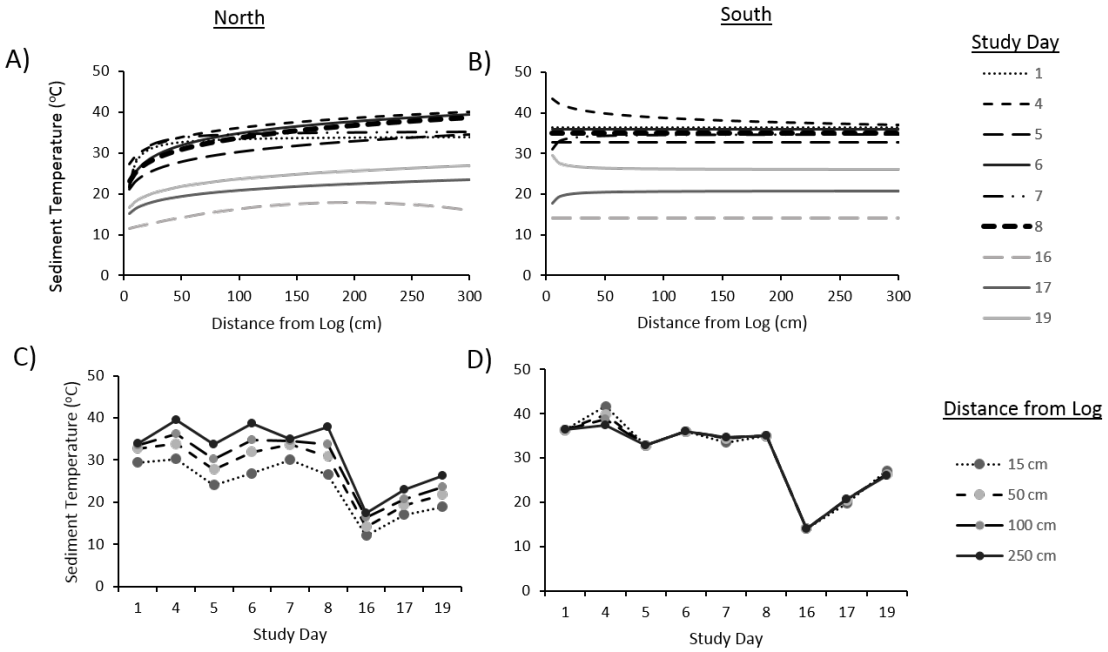

Figure 3.6: The T_S measured along transects of the repeated log each study day. Graphs A and C show transects measured to the north of the repeated log and graphs B and D show transects measured to the south of the repeated log. Graphs C and D show T_S measured at four distances of 15 cm, 50 cm, 100 cm and 250 cm from the log repeated for each study day measured. See table 2.1 for relation of study day to date.

3.2.1.3 Evaporation Rate

Overall, E was smaller near the log for most north transects and increased with greater distance. Near the southern edge of the log, E decreased for a majority of transects. The E far from the log was similar on the north and south sides, but E to greater distances north continues to increase at a larger rate with increased distance compared to the south.

Within-day variability The E to the north is lower near the log during all times except 17:06, which is consistently low for all distances (Figure 3.7). Decreases in E appear to be directly related to reduced incoming direct solar radiation from shade. This shade did not extend past the 30 cm north measurement for any time of day except 17:06, which was in full shade because the sun set behind the valley wall. This is likely why this transect was consistently low for all distances.

To the south, E remains consistent over all distances for each time, except for a slight increase at 15:20 near the south edge of the log (Figure 3.7 B, D). It is not apparent why E decreased near the log at this time or why this decrease did not occur at other times, but suggests that there is possibly an effect of the log on E to the south. However, it is also possible that this could be due to an anomalous data point. Far from the log, southern transects in the morning and early afternoon have values roughly equal to or less than the E modeled to the north, suggesting a possible log effect on E on the leeward side of the log at some times that acts similarly over all distances to the south. This effect is seen at 9:28, 12:30 and 13:33, which are the three earliest times measured within August 21, 2015.

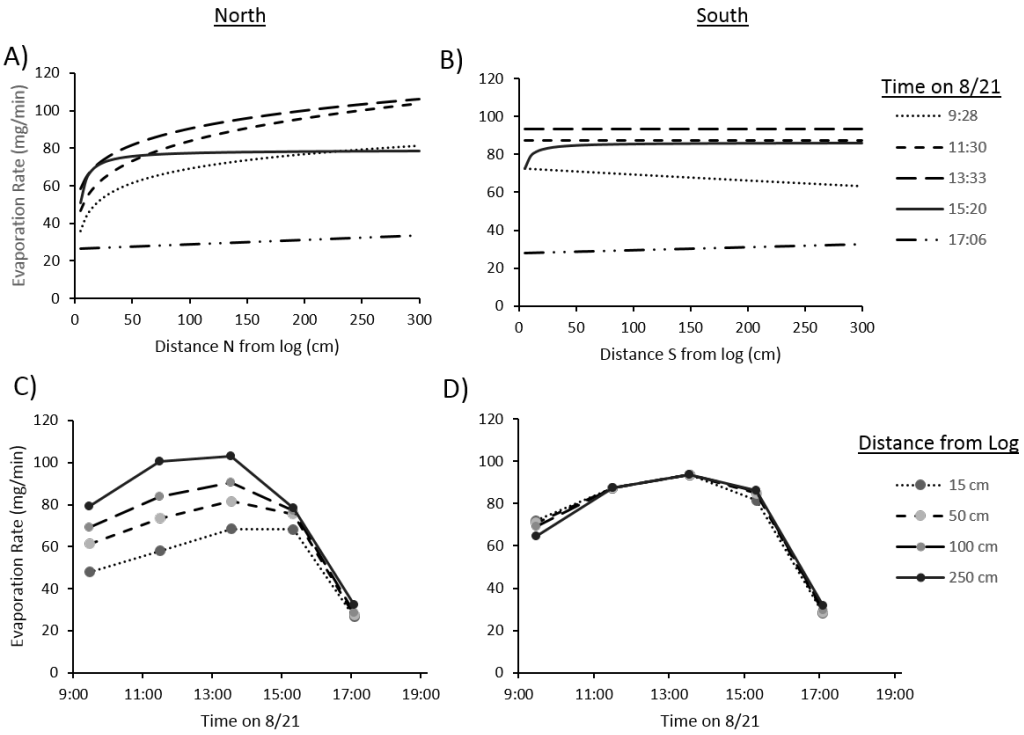

Figure 3.7: Selected curves to represent transects for 5 measured times of day on August 21, 2015 of E. Graphs A and C represent transects measured to the north of the repeated log and graphs B and D represent transects measured to the south of the repeated log. Both graphs A and B contain a single line generated for that transect at 9:28, 11:30, 13:33, 15:20 and 17:06 measured times. Graphs C and D show E modeled by the regressions at four distances of 15 cm, 50 cm, 100 cm and 250 cm from the log repeated five times on August 21, 2015.

Among-day Variability The patterns observed to the north of the log among days were similar in shape to patterns observed within August 21, 2015 (Figures 3.7 A and 3.8 A). The log has a possible effect on E near the log shown by a slight decrease in E within 25 cm.

The ranges of E to the south are similar to the north of the log (Figure 3.7 A and B). Also similar to north transects, E did not vary much within each transect for distances greater than 50 cm from the log. Some south models describe decreased (up to approximately 50%) E within 25 cm of the south edge of the log (Figures 3.7 B, and 3.8 B).

Among days, ranges of E to both the north and south of the repeated log are greater at all distances compared to within a day on August 21, 2015. Similar to T_S, the additional variable of day during the study period is added to the varying times of day and causes an increased range of results modeled for E. This suggests that the E is affected by both time of day and day during this study.

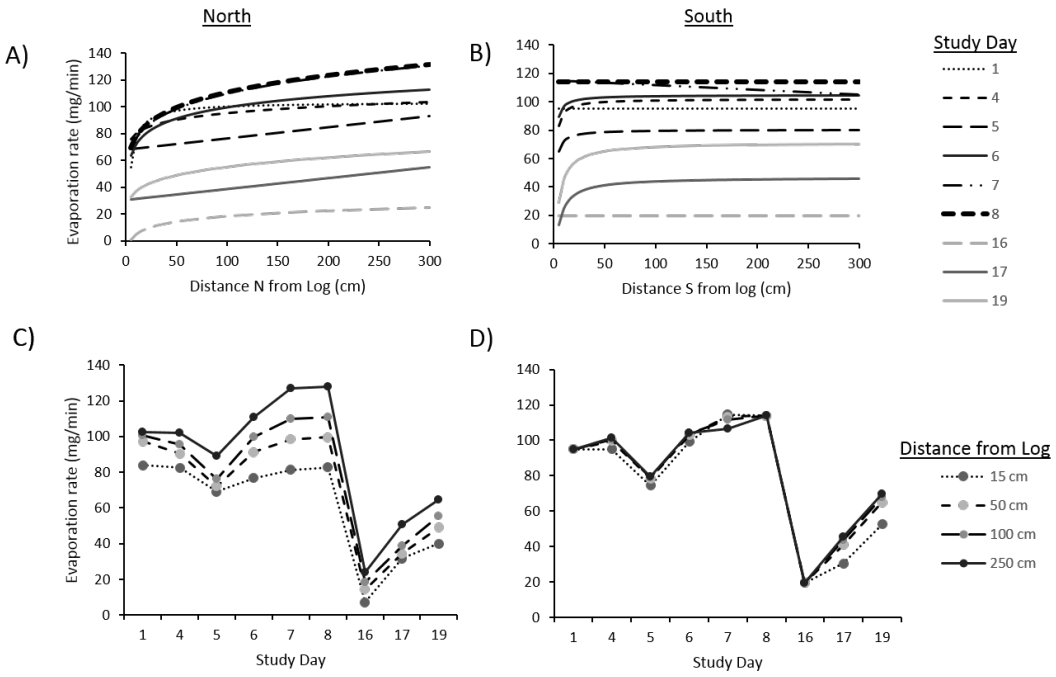

Figure 3.8: The E (mg water loss per minute) (mg/min) measured along transects of the repeated log each study day. Graphs A and C show transects modeled to the north of the repeated log and graphs B and D show transects modeled to the south of the repeated log. Graphs C and D show E modeled values at four distances of 15 cm, 50 cm, 100 cm and 250 cm from the log repeated for each study day measured. See table 2.1 for relation of study day to date.

3.3 Microclimate Near a Log - Quantitative Evaluation

The multilevel regression analysis of log transects aimed to determine the quantitative relation of microclimate to broader environmental factors within dewatered Lake Mills (objective 3). The analysis had four steps. (i) Level 1 regression models fit microclimate as a function of distance and direction from a log, with equation coefficients developed for each of multiple transects. Typical equation coefficients were maximum value of the microclimate variable in the transect (maxV), maximum magnitude of the log's effect (maxeffect), and the distance of the log effect, with distance to half maximum effect as the analyzed variable (dhalfmax). (ii) Level 2 regression models fit level-1 equation coefficients as a function of environmental variables. (iii) Model-informing data were compared with predictions from the combined Level 1 and 2 model. Data were from a log repeatedly measured 14 times. (iv) Independent validation were compared with predictions from the combined Level 1 and 2 model. Validation data were from eight other logs, each measured once.

3.3.1 Common Model Regressions

I fit a common model (either two-line segment or average value) to each of the transects to determine the relation of microclimate to broader environmental factors (objective 3) using multilevel modeling. Both curvilinear and common models fit the repeated log data adequately (Tables 3.1, 3.2 and 3.3). Common models for south T_S or E transects were average values across all distances and no adjusted R^2 were calculated. For nine of 30 transects where a two-line common model was fit, the common model fit the data better than the curvilinear model chosen, reflected by greater adjusted r^2 values. Common models fit worse to other transects, but these models were necessary to compare the transects quantitatively.

Table 3.1: A comparison of curvilinear model fit versus selected common model fit used for multiple regression analyses for each repeated log transect measured on August 21, 2015. Common models represented by average value across all distances have no reported adjusted R^2 and show N/A.

Transect	**Time**	**Curvilinear Adj. R^2**	**Common Model Adj. R^2**
N u_{10}	928	N/A	0.753
	1130	0.929	0.858
	1333	0.743	0.682
	1520	0.934	0.900
	1706	0.706	0.357
N T_S	928	0.868	0.847
	1130	0.815	0.633
	1333	0.784	0.915
	1520	0.956	0.841
	1706	0.883	0.952
N E	928	0.784	0.733
	1130	0.899	0.714
	1333	0.736	0.850
	1520	0.369	0.397
	1706	0.373	0.172
S u_{10}	928	N/A	0.412
	1130	0.548	0.364
	1333	N/A	0.040
	1520	0.680	0.601
	1706	N/A	0.331
S T_S	928	N/A	N/A
	1130	0.552	N/A
	1333	0.709	N/A
	1520	0.848	N/A
	1706	0.849	N/A
S E	928	0.454	N/A
	1130	N/A	N/A
	1333	N/A	N/A
	1520	0.369	N/A
	1706	0.361	N/A

N/A - Average value model; adjusted R^2 were not calculated

Table 3.2: A comparison of curvilinear model fit versus selected common model fit used for multiple regression analyses for each northern repeated log transect other than those measured on August 21, 2015. Common models represented by average value across all distances have no reported adjusted R^2 and show N/A. The transect measured on day 16 was excluded from analysis with common models because no model could be fit.

		North	
Variable	**Study Day**	**Curvilinear Adj. R^2**	**Common Adj. R^2**
u_{10}	1	0.835	0.708
	4	0.938	0.829
	5	0.969	0.978
	6	0.811	0.744
	7	0.966	0.910
	8	0.845	0.946
	16	N/A	**
	17	0.635	0.864
	19	0.937	0.966
T_S	1	0.963	0.916
	4	0.800	0.804
	5	0.902	0.763
	6	0.833	0.952
	7	0.809	0.948
	8	0.897	0.856
	16	0.796	**
	17	0.944	0.871
	19	0.946	0.850
E	1	0.865	0.778
	4	0.481	0.358
	5	0.484	0.732
	6	0.868	0.702
	7	0.853	0.826
	8	0.881	0.790
	16	0.725	**
	17	0.781	0.265
	19	0.705	0.615

N/A - Average value model; adjusted R^2 were not calculated
** - transect was excluded from analysis

Table 3.3: A comparison of curvilinear model fit versus selected common model fit used for multiple regression analyses for each southern repeated log transect other than those measured on August 21, 2015. Common models represented by average value across all distances have no reported adjusted R^2 and show N/A. The transect measured on day 16 was excluded from analysis with common models because no model could be fit.

		South	
Variable	**Study Day**	**Curvilinear Adj. R^2**	**Common Adj. R^2**
u_{10}	1	0.874	0.204
	4	0.930	0.298
	5	0.585	0.504
	6	0.677	0.777
	7	0.693	0.597
	8	0.680	0.595
	16	0.664	**
	17	N/A	0.499
	19	0.525	0.528
T_S	1	N/A	N/A
	4	0.884	N/A
	5	N/A	N/A
	6	N/A	N/A
	7	0.272	N/A
	8	N/A	N/A
	16	N/A	**
	17	0.746	N/A
	19	0.331	N/A
E	1	N/A	N/A
	4	0.483	N/A
	5	0.348	N/A
	6	0.272	N/A
	7	0.197	N/A
	8	N/A	N/A
	16	N/A	**
	17	0.811	N/A
	19	0.813	N/A

N/A - Average value model; adjusted R^2 were not calculated
** - transect was excluded from analysis

3.3.2 Multilevel Regression Modeling

3.3.3 North Wind Speed

3.3.3.1 Repeated Log-Derived Model

The wind speed at 10 cm height (u_{10}) to the north of the repeated log is a function of $\bar{u}_{100}$ and distance north of the log in cm (Table 3.4). I expected this result because u at different heights are known to be related by empirical formulas and because barriers, such as logs affect wind speeds locally, but the effect declines as distance from the barrier increases (Grace, 1977; Rosenberg et al., 1983; Jones, 2013).

Table 3.4: Wind speed at 10 cm height (u_{10}, m/s) as a function of distance from log and local weather variables measured at or near Lake Mills, WA. Input data were transects of the repeated log over the entire study period (n=13).

Wind speed at 10 cm height (u_{10}), north side

$u_{10,North} = min((maxV - maxeffect) + d(\frac{maxeffect}{2(dhalfmax)}), maxV)$

where:	adjusted r^2	n (transects)
$maxV = 0.088 + 0.599\bar{u}_{100}$	0.818	13
maxeffect $= 0.197 + 0.489\bar{u}_{100}$	0.49	13
dhalfmax = 52	-	13

d = distance (cm) from log, (5-300 cm)
$\bar{u}_{100}$ = average wind speed (m/s) at 1 meter height, (1.3 - 9.8 m/s)

Wind speed at 10 cm height (u_{10}), south side

$u_{10,South} = min((maxV - maxeffect) + \frac{d(maxeffect)}{2(dhalfmax)}, maxV)$

where:	adjusted r^2	n (transects)
$maxV = e^{0.585 - 1.840\frac{1}{\bar{u}_{100}}}$	0.808	13
maxeffect $= e^{0.441 - 1.518\frac{1}{\bar{u}_{100}}}$	0.369	13
dhalfmax = 36	-	13

d = distance (cm) from log, (5-300 cm)
$\bar{u}_{100}$ = average wind speed (m/s) at 1 meter height, (0.58 - 4.4 m/s)

Both maxV and maxeffect of north u_{10} increase linearly with $\bar{u}_{100}$, but dhalfmax is a constant in this model, suggesting that the distance of the log effect is always the same. The dhalfmax in this model is 52 cm, implying that the distance of the log effect is approximately 104 cm, which is roughly 1.4 times the repeated log's diameter (measured by log height). This is somewhat less than the 2 to 5 times the height of the barrier object reported by Brandle et al. (2006).

A compound regression and a power regression of maxV with $\bar{u}_{100}$ were usable regressions, but decreased the fit of the overall model of north u_{10} for the transect.

To validate, this model was used to predict the u_{10} along transects of other (non-repeated) logs measured in the former Lake Mills area during this study, then modeled values were plotted against measured values for the model-informing repeated log data (Figure 3.9 A) and model-validating other log data (Figure 3.9 G). Under ideal conditions, the slope of the actual versus predicted line would be 1. For the model-informing data, the slope was close to 1, but for the validation data the slope was much less than 1 indicated by a t test. Therefore one or more factors, or the magnitude of their effects differ between the repeated log and the other logs. Consequently, this model is not useful for use to predict u_{10} to the north of other logs. The greatest difference between the properties of the repeated log and of the other logs in the study is location. The repeated log is on the northernmost edge of the study site and therefore the most windward log of all logs in the October 2014 log drop site (Figure 2.3). The wind to the north side of the repeated log is likely more laminar than the other logs sampled because there were no barriers to wind within 10 meters and therefore there was little friction alter air flow (Grace, 1977).

This model describes a maximum decrease of 2.3 m/s near the north of the log, which, at maximum $\bar{u}_{100}$ would result in an 85% reduction in u_{10} from a maxV of 2.7 m/s. This likely would reduce vegetation stress, but the impact of this reduction would depend on plant species (Wadsworth, 1959; Grace, 1977).

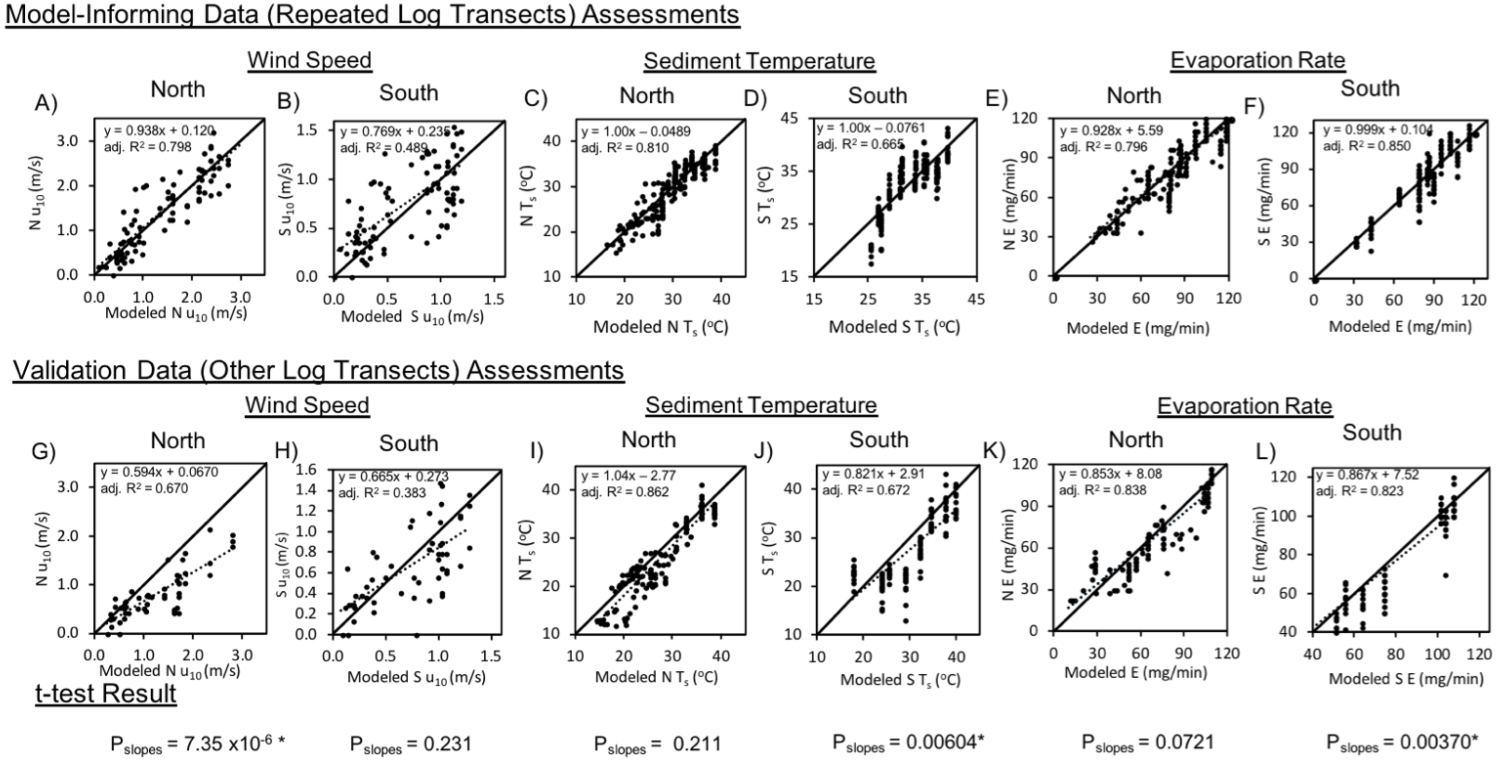

Figure 3.9: Model regression fits to model-informing (repeated log) data and validation (other log) data are shown here for each transect. Modeled values from chosen multiple regression equations are plotted on the x axis and measured data are plotted on the y axis for each graph. Graphs A-F are regression fits with the repeated log data (model-informing data) and graphs G-L are regression fits with data from other logs in the October 2014 log drop area (validation data). The bold black line in each graph represents the ideal regression with a slope of 1 and an intersect of 0. Dashed lines represent the actual linear regressions of modeled data to measured data in each graph. P values from t tests compare the slopes of the regression lines for model-informing and validation data for each transect variable (the two fits above each P value). * indicates a significant t test result ($P < 0.050$)

3.3.3.2 North Wind Speed Other Log-Derived Model

To determine the possible factors that affect the u_{10} to the north of the other logs sampled, the other logs' data were used as input to create another multilevel regression model with maxV, maxeffect and dhalfmax. In this analysis, I included distance to nearest log to the north and number of logs within 25 meters north, as well as the weather variables $\bar{u}_{100}$, and radiation variables R_S, $R_{S,2h}$ and $R_{S,4h}$ as possible regressors of u_{10} to the north of the logs. The sample size of logs measured was too low to both create and validate the model. This model requires validation before use to predict u_{10} to the north of logs, but is presented here as a possible model that is more reliable than the one generated from repeated log data for logs that are not the most windward log. This model also explores the possible differences in factors affecting the repeated log u_{10} and the other logs' u_{10} to the north.

Table 3.5: Wind speed at 10 cm height (u_{10}, m/s) as a function of distance from log and local environmental factors derived from other log data.

Wind speed at 10 cm height (u_{10}), north side

$u_{10,North} = min((maxV - maxeffect) + d(\frac{maxeffect}{2(dhalfmax)}), maxV)$

where:	adjusted R^2	n (transects)
maxV $= 0.538\bar{u}_{100} - 0.456$	0.681	8
maxeffect $= 0.871$	-	8
dhalfmax $= 55.8$	-	8

d = distance (cm) from log, (5-300 cm)
$\bar{u}_{100}$ = average wind speed (m/s) at 1 meter height, (2.2 - 4.5 m/s)

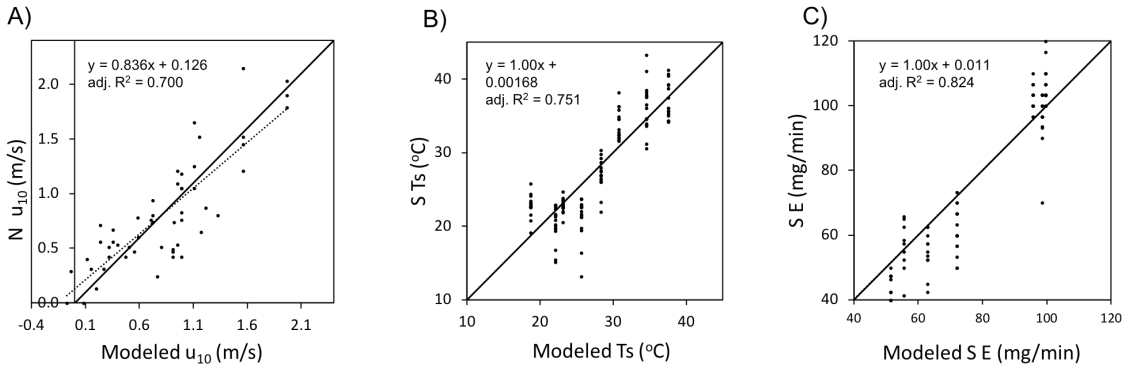

Figure 3.10: Modeled values calculated from the other-log generated model versus measured values for north wind speed at 10 cm height (A), south sediment temperature (B) and south evaporation (C). There were not enough data to create and also validate these models. The equation for the trend line is presented with the adjusted R^2 and the bold diagonal line represents an ideal one to one fit between modeled and measured values. Trend lines for (B) and (C) are present, but not visible because they are hidden by the bold ideal fit line.

The best model fit to the other logs was also a function of distance north from the log and $\bar{u}_{100}$, but with a few key differences (Table 3.5). The greatest difference between this model and the repeated log-generated model is the relationship of maxV with $\bar{u}_{100}$. In both models, u_{10} increases linearly with $\bar{u}_{100}$, but in this model, the intercept of this regression is lower (-0.456 compared to the repeated model maxV intercept 0.088) (Tables 3.4 and 3.5). This suggests that u_{10} to the north of these other logs is always slower than to the north of the repeated log, because the other logs are shielded by upwind logs. The range of $\bar{u}_{100}$ measured around the other other logs is similar to the range measured at the repeated log. This suggests that the upwind logs are not affecting wind at 1 m height.

This model describes a maximum decrease of 0.87 m/s near the north of the log, which may reduce vegetation stress, but the impact of this reduction would depend on plant species and the value of $\bar{u}_{100}$ (Wadsworth, 1959; Grace, 1977). The maximum modeled maxV is 2.0 m/s, so this effect would reduce u_{10} by 44%.

The dhalfmax for the other log-derived model (55.8 cm) was similar to that of the repeated log-derived model (52 cm). Because the logs used to create this model varied in height (diameter), a constant value for dhalfmax is unexpected. The distance of wind shelter is known to be a function of the height of the barrier object (Skidmore

and Hagen, 1973; Grace, 1977; Brandle et al., 2006; Mayaud et al., 2016). Based on conceptual knowledge of u, the log's effect on the u_{10} is highly dependent on the $\bar{u}_{100}$ (Rosenberg et al., 1983). However, $R_{S,2h}$ and $R_{S,4h}$ were also included as possible regressors for maximum u_{10}, maxeffect and dhalfmax. This energy input into the system may affect u_{10} by causing convective air flow near the surface of the sediment (Rosenberg et al., 1983). These regressions were insignificant for the maximum u_{10} and maxeffect values, but resulted in a significant regression equation including both $R_{S,2h}$ and $R_{S,4h}$ data with dhalfmax. This regression was not included in the overall model for predicting u_{10} to the north, but it is worth mentioning that this radiation energy input into the system may affect the distance to the north where a log may have an effect on u_{10}, but likely does not affect the magnitude of speeds or effects the log has on u_{10}.

3.3.4 South Wind Speed

Similar to u_{10} to the north, u_{10} to the southern, leeward side of a log is also a function of distance from the log in cm and of $\bar{u}_{100}$ (Table 3.4). Again, this is consistent with known empirical relationships between u at various heights from the ground surface and influences of barriers on wind speed (Skidmore and Hagen, 1973; Grace, 1977; Rosenberg et al., 1983; Brandle et al., 2006; Jones, 2013; Mayaud et al., 2016).

MaxV in this model is related to $\bar{u}_{100}$ with an S curve. As in the linear models of maxV to the north, increases in $\bar{u}_{100}$ lead to increases in u_{10}. The maximum maxV that can be modeled with this equation is 2.7 m/s

The maxeffect in this model is also related to $\bar{u}_{100}$ with an S curve, whereas $\bar{u}_{100}$ increases, the windbreak effect of the log also increases. This relationship is not as strong as the maxV relationship (max effect adjusted R^2 0.369 versus maxV adjusted R^2 0.808), but it suggests that the log can continue to provide shelter, even as u above may be increasing. Based on maximum $\bar{u}_{100}$ values, the maximum effect to the south is 1.1 m/s. This would reduce the maximum modeled maxV by 41%.

The dhalfmax in this model is represented by a constant value of 36 cm. This

projects to an approximate distance of log shelter effect of 72 cm, which is approximately one log diameter and about equal to the height of the log as a barrier. Though this is the measured windbreak distance in this study, more information is needed to predict the effect this would have on individual plants and plant species nearby to logs. This windbreak distance is surprisingly low compared to literature that suggests that the wind-break distance of barriers is between two and nine times the height of the barrier (Woodruff et al., 1963; Grace, 1977; Fryrear and Skidmore, 1985; Brandle et al., 2006; David et al., 2016; Mayaud et al., 2016). This range in distances of effect is created by the range in porosity of barriers in these studies. Barriers with low porosity, like the logs in this study, have less effect on the wind and do not reduce wind speeds at greater distances as well as some more porous barriers because the lack of porosity causes increased turbulence in the lee (Rosenberg et al., 1983). I was unable to measure data points to nine times the height of the log, but only to approximately 3.5 times. Logs in the October 2014 log drop area were too closely spaced and I would not have been able to discern between a potential windbreak effect to the south of a log and to the north of another log. Perhaps I am only measuring the wind-break affected region to the south of the log and am not observing the u_{10} increase back to the true maximum. Curvilinear models of u_{10} show that u_{10} is always slowed to the south compared to the north at all distances observed and u_{10} never reaches the maximum observed on the windward side (Figures 3.3 and 3.4). This also suggests that all distances measured to the south of logs are experiencing the log's effect of slowed u_{10}.

The slope of the model fit regression shows that this model is biased towards underestimating $u_{10,South}$ (i.e. - slopes were less than 1) (Figure 3.9 B, H). The u_{10} appears highly variable, because the range of u_{10} measured to the south is much smaller compared to the north side of logs. A t test of model fit regression slopes determined that this model applies similarly for u_{10} for all logs sampled in the former Lake Mills October 2014 log drop area ($P > 0.05, P = 0.231$).

In addition to $\bar{u}_{100}$, maxV, maxeffect and dhalfmax for south u_{10} were also re-

gressed with $R_{S,2h}$, but regressions were insignificant. Therefore, if $R_{S,2h}$ is an indicator of convective air movement, then this air movement is likely not affecting u_{10} values to the south, similar to the north repeated log u_{10} model.

3.3.5 North Sediment Temperature

The T_S modeled to the north of the log is a function of T_a during the time transected (^{o}C) and two and four-hour cumulative radiation input (Whm^{-2}) (Table 3.6). The maxV is a linear function of T_a, while maxeffect is a function of $R_{S,2h}$ and dhalfmax is a function of $R_{S,4h}$.

The the maxV linear regression with T_a is slightly misleading, because change T_a likely is not causing changes in T_S, but is a good indicator of T_S values (Adeniyi and Nymphas, 2011; Mutiibwa et al., 2015). Data for T_a is often readily available and predictable for restoration and study sites. Therefore, though T_a may not have any conceptual basis for causation of changes in T_S, using T_a as input for T_S models may be useful still. Adeniyi and Nymphas (2011) found that T_a and soil surface temperatures in a tropical region in Nigeria were related linearly with R^2 values ranging from 0.97 to 0.99. That is to say, if T_a is increased, the value of T_S is likely increased, but both increases are likely caused by similar, additional physical factors, such as radiation variables: R_S, $R_{S,2h}$ and $R_{S,4h}$, though no significant regressions of T_S were found with these variables.

Table 3.6: Sediment temperature (T_S, ^{o}C, at 3 cm depth) as a function of distance from log and local weather variables measured at or near Lake Mills, WA. Input data were transects of the repeated log over the entire study period (n=13).

Sediment temperature (T_S, ^{o}C, at 3 cm depth), north side

$T_{S,North} = min((maxV - maxeffect) + d(\frac{maxeffect}{2(dhalfmax)}), maxV)$

where:	adjusted R^2	n (transects)
$maxV = 1.27T_a + 2.67$	0.736	13
maxeffect $= e^{0.744101ln(R_{S,2h})-2.87}$	0.291	13
dhalfmax $= e^{5.65-0.000945(R_{S,4h})}$	0.372	13

d = distance (cm) from log, (5-300 cm)
T_a = average air temperature (^{o}C) at 1 meter height, (14.2-28.4 ^{o}C)
$R_{S,2h}$ = 2 hour cumulative solar radiation (Whm^{-2}), (788.-1640 Whm^{-2})
$R_{S,4h}$ = 4 hour cumulative solar radiation (Whm^{-2}), (1190- 3110 Whm^{-2})

Sediment temperature (T_S, ^{o}C, at 3 cm depth), south side

	adjusted R^2	n (transects)
$T_{S,south} = 68.16 - 811.15\frac{1}{T_a}$	0.715	13

where:
T_a = average air temperature (^{o}C) at 1 meter height, (14.2-28.4 ^{o}C)

The maxeffect is a power function of $R_{S,2h}$, indicating that when there is more radiation in the previous two hours, the effect that the log has on decreasing T_S is greater. This likely means that greater recent radiation results in a greater difference between the shaded distances closer to the log and sunnier distances further from the log. Increased radiation input increases sediment temperature (Rosenberg et al., 1983; Geiger et al., 2009; Jones, 2013). Greater $R_{S,2h}$ amplifies the differences between sun and shade differences and therefore a greater maxeffect is observed. An adjusted R^2 of 0.291 indicates that this relationship between $R_{S,2h}$ and maxeffect is somewhat weak, but including this relationship in the overall model of north T_S improves the model fit to measured data.

The dhalfmax is a function of $R_{S,4h}$, where an increase in $R_{S,4h}$ results in an increase in dhalfmax. This is also probably shade-related like maxeffect. Greater $R_{S,4h}$ occur later in the day when there has been more radiation in the previous four hours (Figure 3.1). These times of day also create longer shadows from the log to the north. The $R_{S,4h}$ may be a weak (adjusted R^2 0.372) proxy for shadow distance from logs in this site.

Insignificant t test results for model-fit slopes suggest that there is no difference in model fit between the repeated log and other logs (P = 0.211) (Figure 3.9 C, I). This, along with adjusted R^2 values of 0.810 and 0.862, and slopes of 1.00 and 1.04 for repeated log and validation data, respectively, suggest that this model works well for this log population. Therefore the factors that affect T_S to the north of the repeated log are the same as the factors that affect it north of the other logs in the October 2014 log drop area.

Maxeffect also had other significant regressions of $R_{S,2h}$ and $R_{S,4h}$, but these resulted in worse fits for the overall model. MaxV was only a function of T_a and dhalfmax was only a function of $R_{S,4h}$, though several significant regression types were found for each of these. These also resulted in worse model fit.

3.3.6 South Sediment Temperature

3.3.6.1 Repeated Log-Derived Model

The T_S to the south of the log was not a function of distance, and the average value of T_S south of the log at all distances is the best model (Table 3.6). The average value of T_S to the south of logs is a function of T_a.

As discussed with the north T_S maxV regression, T_a is not necessarily a cause of T_S, but is a variable that often changes with and is used as an indicator for T_S (Adeniyi and Nymphas, 2011; Mutiibwa et al., 2015). The $R_{S,4h}$ is more likely a variable that directly causes changes in T_S based on conceptual models of the radiation balance (Rosenberg et al., 1983; Geiger et al., 2009; Jones, 2013). I determined other significant regression functions for south T_S including $R_{S,4h}$, $R_{S,2h}$ and other regressions of T_a, but these did not improve the overall fit of the model.

3.3.6.2 South Sediment Temperature Other Log-Derived Model

The t test result between slopes of repeated log data fit and other-log validation data fit support the conclusion that there is a difference between the model fit to validation data (P = 0.00604) (Figure 3.9 D, J). Therefore the factors that affect the T_S to the south of the repeated log are different from the factors that affect it south of the other logs measured.

To determine the possible factors that affect the T_S to the south of the other logs sampled, the other logs' data were used as input to create another regression model. The sample size of logs measured was too low to create a reliable model of T and also be able to validate the model with additional data. This model requires validation before use to predict T_S to the south of logs, but is presented here as a possible model.

The best model fit to the other logs was also a function of T_a, but with a few differences (Table 3.7). This model is a linear function, instead of the inverse function created using the repeated log data. The slope of sampled versus modeled values is 1 (Figure 3.10 B). This model may be slightly different than the repeated log model

due to the increased diversity of size, location and orientation of the other logs.

Table 3.7: Sediment temperature at 3 cm depth (^{o}C) to the south of a log as a function of local weather variables measured at or near Lake Mills, WA derived from other-log data.

Sediment temperature (T_S, ^{o}C, at 3 cm depth), south side		
	adjusted R^2	n (transects)
$T_{S,south} = 1.507T_a - 5.581$	0.814	8

where:
T_a = average air temperature (^{o}C) at 1 meter height, (16.1-28.6 ^{o}C)

3.3.7 North Evaporation Rate

The E (mg water loss per minute) (mg/min) to the north of a log is a function of ρ, R_S, and distance from the north log edge (Table 3.8). The maxV in this model is a multiple regression function of ρ and R_S. Maxeffect is represented by an S function of R_S. The dhalfmax in this analysis did not regress with any environmental variables and are represented by the average value.

Based on conceptual models of evaporation, wind may also affect evaporation in addition to ρ and R_S, but $\bar{u}_{100}$ did not result in any significant regressions for any of these parameters (Penman, 1948; Rosenberg et al., 1983; Shuttleworth, 1993). It is possible that wind may be affecting this system, but with these data, the ρ and R_S are the strongest influence on these patterns of E to the north of logs.

Table 3.8: Evaporation Rate (E, mg/min) as a function of distance from log and local weather variables measured at or near Lake Mills, WA. Input data were transects of the repeated log over the entire study period.

Evaporation Rate (E, mg water loss per min, mg/min), north side

$E_{North} = min((maxV - maxeffect) + d(\frac{maxeffect}{2(dhalfmax)}), maxV)$

where:	adjusted R^2	n (transects)
$maxV = 31.024\rho + 0.08164R_S - 17.746$	0.797	11
maxeffect $= e^{4.757 - 729.167\frac{1}{R_S}}$	0.446	11
dhalfmax $= 26.25$	-	11

d = distance (cm) from log, (5-300 cm)
ρ = vapor pressure deficit (kPa)*
R_S = solar radiation (Wm^{-2})*

Evaporation Rate (E, mg/min), south side

	adjusted R^2	n (transects)
$E_{South} = 29.740\rho + 0.08354R_S - 17.654$	0.890	12

where:
ρ = vapor pressure deficit (kPa)*
R_S = solar radiation (Wm^{-2})*

* see Figure 3.11 for range of acceptable values

Other models have used regression modeling based approaches to determine which variables have greater influence on E. Tabari et al. (2010) found that wind speed and T_a were the most important environmental variables to predict evaporation in a semi arid region in western Iran, using a different modeling technique. Kim et al. (2013) used various modeling techniques and combined varying environmental factors for predicting daily pan evaporation at two weather stations in semi-arid South Korea and found that the environmental variables that were best predictors for pan evaporation varied for the two weather stations. Pan evaporation at both sites were best predicted by temperature-based models than sunshine duration or radiation-based models but

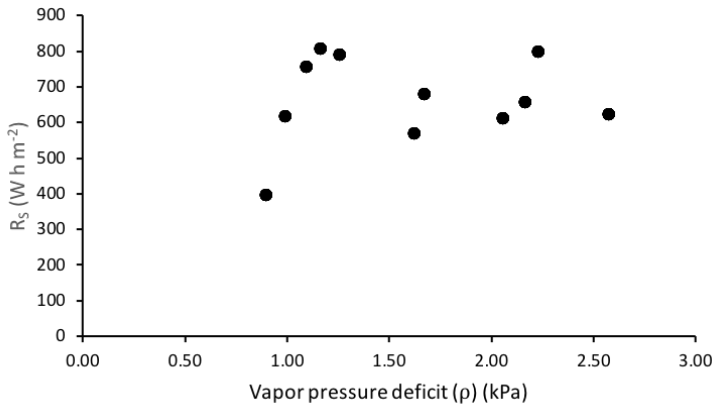

Figure 3.11: The acceptable values of ρ to be used with radiation values (R_S) in models of E. This universe of data is used instead of acceptable ranges due the models containing multiple regressions. Where ρ and R_S fall within the respective cloud, the models should be applicable.

models that combined temperature, radiation, sunshine duration and wind speed predicted best for both sites overall. In the same climatic region as the Elwha, Jassal et al. (2009) found monthly evapotranspiration from Pacific Northwest Douglas Fir stands to be strongly correlated to montly net radiation, T_a and daytime ρ, but did not determine the relative importance of those three or compare wind speeds. However, it is difficult to determine the relative influence of physical and environmental factors from biological factors within plants on evapotranspiration (Tan and Black, 1976). The relative influence of weather predictor variables in evaporation modeling is site-dependent and the Elwha Oct 2014 log drop site is most heavily influenced by ρ and R_S.

This model fit well to both the model-informing repeated log and other validation logs' data with adjusted R^2 values of 0.796 and 0.838, respectively (Figure 3.9 E, K). These suggest that this is a good model for north E in the Elwha October 2014 log drop site. A t-test analysis of the model fit slopes between modeled and measured E values show that there is no difference in the way the model fits either data set (P = 0.0721). Therefore the factors that affect E to the north of the repeated log are likely the same as other logs in the validation data. This model is acceptable to use to predict northern E for logs of variable size, orientation and location within the October 2014 log drop area.

3.3.8 South Evaporation Rate

3.3.8.1 Repeated Log-Derived Model

The E to the south was not a function distance south of the log, and the average value of E over all distances south is the best model of south E (Table 3.8.) The E to the south is a function of ρ and R_S, similar to the regression of $maxV$ for north E. Similar coefficients in both regressions suggest that $maxV$ behaves similarly to E at all distances measured to the south and therefore there is no log effect to the south. The E at all distances to the south are similar to those at greater than approximately 55 cm north.

Similar to the model of northern E, the lack of $\bar{u}_{100}$ in significant regressions with E_{South} is suggests that ρ and R_S are the greatest driving factors of E. The relative influence of environmental factors is site dependent (Jassal et al., 2009; Tabari et al., 2010; Kim et al., 2013).

3.3.8.2 South Evaporation Rate Other Log-Derived Model

A significant t test result (P = 0.00370) between the slopes of the model-fit regressions on repeated log data and validation data supports the conclusion that there is a difference in how the model fits the two data sets and therefore the factors that affect the E to the south of the repeated log are different from the factors that affect it south of the other logs in the validation data (Figure 3.9 F, L).

To determine the possible factors that affect the E to the south of the other logs sampled, the other logs' data was used as input to create another regression model. The sample size of logs measured was too low to create a reliable model of E and also be able to validate the model with additional data. This model fits well to other log measured values, but requires validation before use to predict E to the south of logs, but is presented here as a possible model (Figure 3.10 C).

The best model fit to the other logs was also a function of ρ and R_S, but with coefficients less than those determined for the repeated-log derived model (Table 3.9).

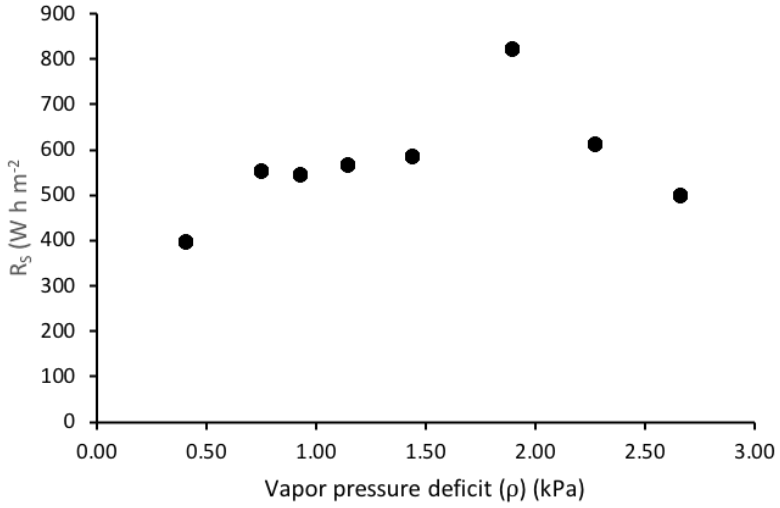

Figure 3.12: The acceptable values of ρ to be used with radiation values (R_S) in the other log-derived south E model. This universe of data is used instead of acceptable ranges due the model being a multiple regression model. Where ρ and R_S fall within the respective cloud, the model should be applicable for use.

These decreased coefficients suggest that the E to the south of the other logs in the validation data is just lower than the repeated log. This mimics the pattern of u_{10}, where u_{10} was slowed to the south at all distances (Figures 3.3 and 3.4). Though no significant regressions of $\bar{u}_{100}$ were found for south E, it is possible that the slowed u_{10} to the south of logs may lead to decreased E at this height.

Table 3.9: Evaporation rate (E, mg/mL) to the south of a log as a function of local weather variables measured at or near Lake Mills, WA derived from other-log data.

Evaporation Rate (E, mg/min), south side		
	adjusted R^2	n (transects)
$E_{South} = 26.488\rho + 0.066180R_S - 5.172$	0.883	8

where:

ρ = vapor pressure deficit (kPa)*
R_S = solar radiation (Wm^{-2})*

* see Figure 3.12 for range of acceptable values

3.3.9 Summary of Influence of Logs on Microclimate

The greatest log effect on u_{10} occurs in the immediate lee (less than 72 cm from the log, on average). The leeward u_{10} remains reduced for all distances from northern, windward u_{10} suggesting that the effect of the northern-most windward log may act over distances greater than 300 cm. The greatest reduction u_{10} occurs near the northern, windward edge of the log (approximately 104 - 112 cm on average). This region of slowed wind speed occurs near a barrier when wind is redirected upward and over the barrier object on the windward side (Rosenberg et al., 1983).

From the windward north to the leeward south, the log slows u_{10} by 50% on average for the repeated log model and 11% for other log model (Figure 3.13). The maximum u_{10} on the windward side of the other logs is similar to the maximum u_{10} modeled to the lee of both the repeated log and other logs (using the same model). This suggests that the windward-most log, the repeated log has the most effect on slowing u_{10} for the entire LWD area.

As wind approaches the north edge of a log, it slows starting at about 112 to 104 cm from a log on average. The maximum decrease to the north of the repeated log is 83% on average and 72% to the north of the other logs. Both the north repeated and other log models show a similar minimum u_{10} of 0.33 to 0.34 m/s near the log. The minimum u_{10} near the south, leeward edge of the log is less than the minimum u_{10} on the windward side near the log edge. On average, the decrease from in u_{10} to the immediate south of the log (within an average of 72 cm) is 89% from the maximum values measured at greater distances.

The greatest effect of the log on T_S occurs immediately to the north of the log, on the shaded side (Figure 3.14). Within about 55 cm north on average, T_S decreases 33% from the maximum value modeled at greater distances.

There is a slight decrease in T_S from the north to the south of the other logs (average 14% decrease). However, the maximum value of T_S to the sunny, south side of the repeated log is within 3% the values modeled to the north, suggesting no difference. There is no effect of southern distance from the log on T_S for either the

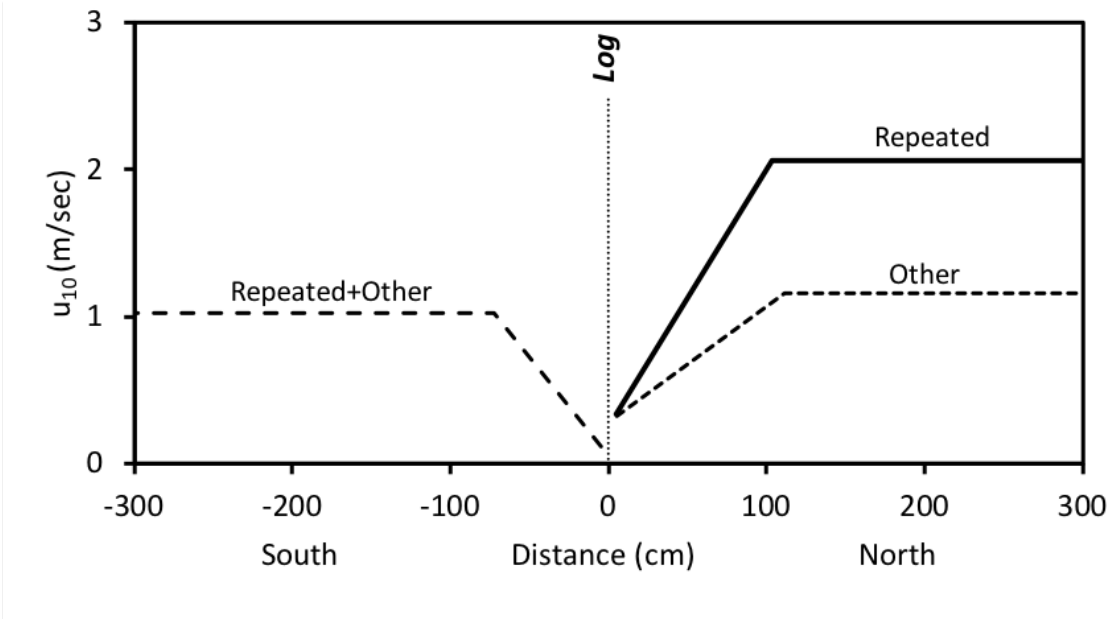

Figure 3.13: Plots of two-line segment models of wind speed at 10 cm height (u_{10}) for repeated and other logs. Lines are based on the average $\bar{u}_{100}$ measurements. The north is the windward side of the log and the south is the lee. Equations for these models can be found in tables 3.4 and 3.5.

repeated or other log models.

The greatest log effect on E occurs to the immediate north of both repeated and other logs, similar to T_S (Figure 3.15). On average, this decrease in E occurs within 52.5 cm and is up to 41% less than E modeled at greater distances. There is no effect of southern distance from the log on E.

The maximum value of E to the north of the repeated log is 1% greater than to the south, indicating little to no log effect between north and south. The maximum value of E to the north of other logs is 15% greater than to the south, suggesting that there may be an effect of the log on E from the north to the south of other logs.

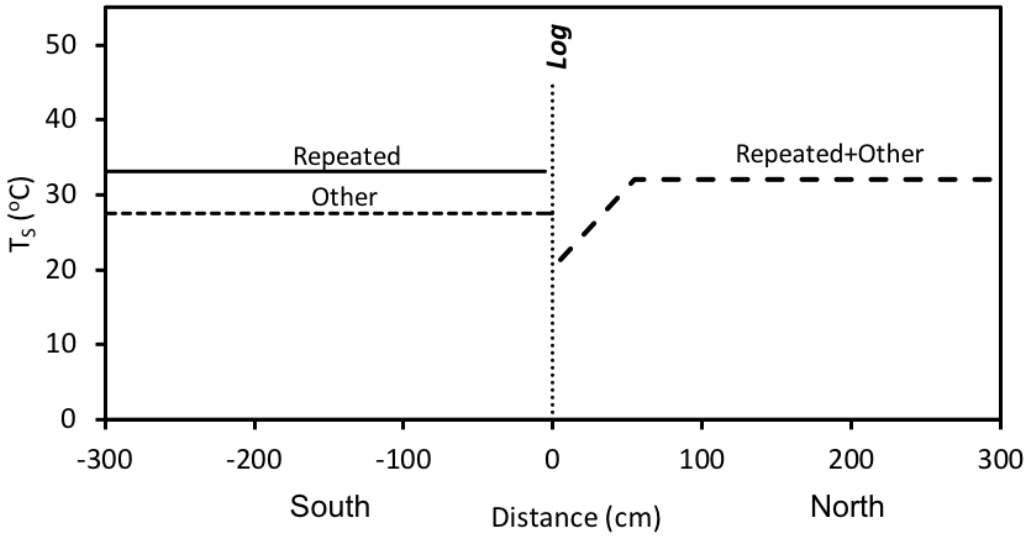

Figure 3.14: Plots of the two-line segment models of north sediment temperature (T_S) and average value models of south T_S based on the average values of air temperature (T_a), and two and four-hour cumulative radiation ($R_{S,2h}$ and $R_{S,4h}$). The north is the shaded side of the log. Equations for these models can be found in Tables 3.6 and 3.7.

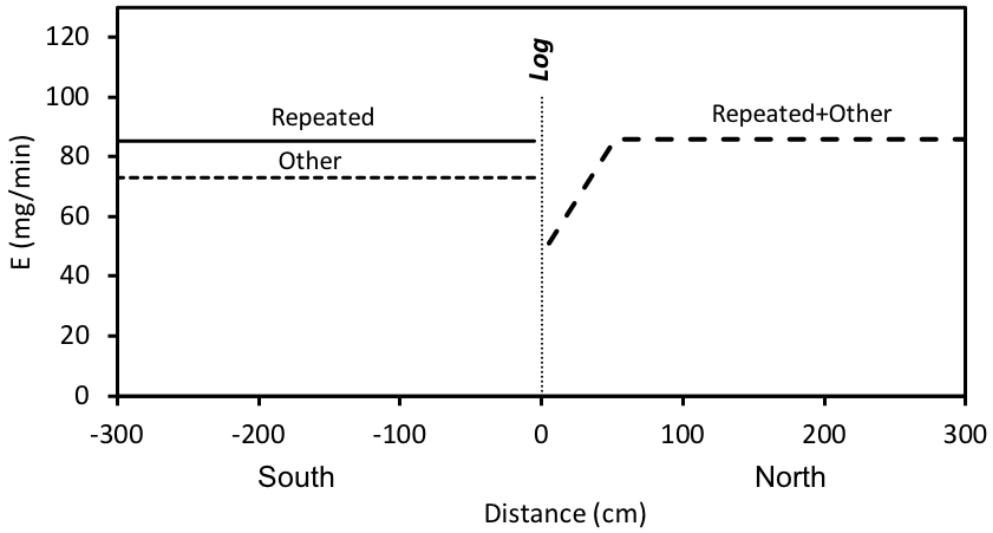

Figure 3.15: Plots of the two-line segment models of north evaporation rate (E) and average value models of south E based on the average values of vapor pressure deficit (ρ) and solar radiation (R_S). The north is the shaded, windward side of the log. Equations for these models can be found in Tables 3.8 and 3.9.

3.4 Log Diversity

Half of the models, south u_{10}, north T_S and north E, did not show a significant difference between the fit to the input data from the repeated log transects and the validation data of the other logs sampled during this study. This suggests that differences in log diameter and orientation are not as important to the effect that logs have on their surrounding microclimate as the overall patterns in the weather for these variables and transects. However, north u_{10}, and south T_S and E results suggest that the factors that drive the microclimate in these transects for the repeated log are different than those that drive the microclimate around the other logs. Other models were created for north u_{10}, and south T_S and E using the other log's data and are described above in Sections 3.3.3.2, 3.3.6.2, and 3.3.8.2. These models aim to describe the external environmental factors that may influence microclimate around these other logs uniquely from the repeated log, but don't investigate the differences in log diameter and orientation.

Barrier height is known to affect the distance of slowed u and also would affect the distance of shadows on sediment surface, possibly affecting T_S and E (Grace, 1977; Fryrear and Skidmore, 1985; Brandle et al., 2006; David et al., 2016; Mayaud et al., 2016). To determine if microclimate models could be improved by accounting for the differing heights of the logs, the regression analysis was repeated for the transects and variables where the two-segment model was used (i.e. - the variable value was a function of distance from the log: North and south u_{10}, north E and north T_S). In this reanalysis, all distances were divided by the diameter of the log and thus transformed into units of 'log heights'. In this study, the logs are assumed to be approximately round and therefore the diameter measured horizontally is assumed to be the height of the log.

When distances were standardized to log diameter units, the changes in model fits compared to models with distances in centimeters were variable (Table 3.10). The distance unit change improved the north T_S model only slightly (by improving intercept closer to 0, and both adjusted R^2 and slope remained approximately the

same), but resulted in a worse fit for north u_{10}, north E and south u_{10}. For north u_{10} and E, adjusted R^2 were reduced, resulting slopes were further from 1 and intercepts were much further from 0. For u_{10} the model remained relatively the same except for a noticeable decrease in R^2. Such variable, and often detrimental effect suggests that the effect of log height is not measurable in the microclimate patterns nearby.

From this analysis, the diversity of logs' orientations and heights in the study area were found to have negligible, non-measurable effect on the patterns of microclimate around the logs. This finding is contradictory to literature about barrier effects (Grace, 1977; Fryrear and Skidmore, 1985; Brandle et al., 2006; David et al., 2016; Mayaud et al., 2016). The input data for the models with distances in log diameters were all collected from the repeated log to mimic the methods for distances in centimeters. However, this means that the input data did not have a diversity of log diameters and any model created from these data would likely miss some of the effect of measuring distances in log diameters. This is likely why using distances diameters has no change on the model fits. Additionally, the range of diameters were controlled to be approximately east-west and therefore there was not much diversity in orientations of the log sample. An increased range of orientations may allow for detection of a log orientation effect on microclimate patterns, if there is an effect.

This study does not address some other aspects of log diversity, including the presence and size of attached root wads and more detail about location such as distance from terrace edge, sediment sizes nearby to the logs and aspect and slope of the location where the log was placed. Further information about the logs could be investigated in further studies of how log diversity affects the log effect on microclimate.

Table 3.10: Model fit change when distances were converted from cm to log diameters. Values are differences between model fit equations and R^2 values for other logs where distances were measured in log diameters and where distances were measured in cm. Green text shows an improvement in model fit parameter, red text shows decrease in regression parameter fit and black text shows neutral change (i.e. - very little change from modeled distances in cm). Net change in model fits (Net Δ) is estimated from changes in the model fit parameters.

		$\Delta adj.R^2$	Δ Slope	$\Delta \lvert Intercept \rvert$	Net Δ
North					
	u_{10}	-0.486	-0.108	2.27	worsens
	T_S	0.0455	0.0554	0.625	improves
	E	-0.340	-0.478	36.6	worsens
South					
	u_{10}	-0.0958	-0.0685	0.0657	worsens

3.5 Potential Effect on Vegetation

For models where a log effect was measured, there may be an impact on vegetation near the log. The potential maximum effects of these logs on microclimate variables is best estimated from the maxeffect in each of the models. This maximum effect only exists at the nearest point to the log edge and the effect decreases as distance from the log decreases, until the maximum value of the microclimate variable is reached (maxV) (Figure 2.6). Models where distance from the log was not a factor do not incorporate a maxeffect parameter and imply that there is no log effect detected in that model. The u_{10} to the north and south, northern T_S and northern E all show a log effect by this measure. Here are the predicted maximum effects that the microclimate manipulation may have on vegetation growth near logs.

To the south of the log, the maximum possible reductions in u_{10} modeled are between 0.5 and 1.3 m/s. Depending on the net u_{10} after the log has slowed u, the reduction in u_{10} could reduce dessication and mechanical damage resulting in loss of biomass (Wadsworth, 1959; Grace, 1977; Grier, 1988). Wadsworth (1959) reported an

optimum wind speed of 0.3 m/s for herbaceous *Brassica napus* (rapeseed), which is lower than the modeled range of reduced u_{10} in this study. Values of reduced u_{10} could range between 0.160 m/s and 0 m/s (Table 3.4). Compare these to the windward maximum u_{10} of 5.95 m/s to 0.867 m/s. The minimum southern u_{10} modeled would be less than optimum for *Brassica napus*, but the optimum u_{10} for native Elwha species, including tree seedlings, are unknown. It is possible that these u are more ideal for native Elwha species, but more information is needed on the relative tolerances of wind (Wadsworth, 1959). However, the maximum u_{10} experienced at greater distances to the north could cause stress and therefore I expect these reductions would be beneficial.

To the north, T_S can be reduced between 2.1 and 2.6 ^{o}C dependent on the $R_{S,2h}$ value (Table 3.6). The maximum possible modeled T_S (based on maxV equation and a maximum T_a of 28.4 ^{o}C) would be 38.7 ^{o}C, which is close to the lower limit of the range of T_a that cause heat damage to temperate plant species (Jones, 2013). This temperature is likely great enough to reduce metabolic rates, though this is dependent on species (Jones, 2013). The extremes of modeled reduced T_S to the north are between 36.6 and 18.1 ^{o}C.

Also to the north, E can be reduced between 19.0 and 47.5 mg/min dependent on values of ρ and R_S (Table 3.8). This would result in a final reduced E of between 96.3 and 23.6 mg/min. This reduction in evaporation stress is also likely significant for plant survival. Reducing evaporative stress in a moisture-limited environment is advantageous for plant growth and survival in Pacific Northwest forests during dry summer months (Waring and Franklin, 1979), but species-specific reactions to this stress reduction are currently unknown, to my knowledge. Reducing Es also likely increases the retention of moisture in the sediment near the log, which would provide less limitation to transpiration and provide a better environment for soil respiration (Cook and Orchard, 2008).

3.6 Model Applications and Limitations

Models of south u_{10}, north T_S and north E are effective for predicting microclimate patterns around LWD in the October 2014 log drop area. However, these models are very limited to the population they may be applied to. If these models were developed with other restoration sites using LWD, and with a greater diversity of log size, orientation, decay class and height off of the ground, the model could be applied to a greater population of LWD and could be used more widely. These models provide the framework for creating more general models of LWD and microclimate. Similar methods could be applied in other regions to create a more comprehensive model. These models are also limited temporally and to the range of environmental conditions in the Elwha watershed during the sampling months in late summer 2015. With more data for other seasons and years, these models could be applied more widely.

The models of north u_{10}, south T_S and south E require validation with more data from other logs before they can even be applied within the October 2014 log drap area. Beyond this validation, these models could also be developed further with more diverse log microclimate data to be applied with a broader scope.

With further development to apply to a broader range of areas and environmental conditions, all of the models developed in this study could be used to quantify potential patterns in microclimate around LWD could inform land managers if placing LWD may be a useful strategy for restoration. It could also inform them where planting and seeding efforts should be focused to maximize the benefit of improved microclimate around already-existing LWD or artificially-placed LWD.

Additionally, all logs sampled in this study were oriented approximately the same direction and were of the same decay class. Wood in a different decay class may have a different effect on the local environment (Gray et al., 2002), separate from the barrier-effect that is described in this study, and any effect of decaying matter on microclimate is not captured by the mathematical models described here. Log orientation and presence of root wads may have large effects on the length of shadows

cast and patterns in wind turbulence and could have larger effects on microclimate than what was observed during this study.

3.7 Future Research

Within the October 2014 log drop area within Lake Mills, the models created in this analysis which describe a distance of log effect could be used to calculate an overall area of log effect surrounding each log to determine the overall area with manipulated microclimate. This may be a more appropriate metric of measuring log effect in some regions and would describe the overall area where plants may have an additional advantage for survival and growth. This would be an approximate area of influence and the degree of influence would depend heavily on daily weather conditions and would not be a consistent amount of effect throughout this defined area of influence. This area of effect would describe the region where a gradient is occurring for each variable influenced by logs.

Measurements on moisture retention in sediments nearby logs would also be useful information in describing more of the soil microclimate that plants may experience. Peters et al. (2008) found increased soil moisture retention 19 days after a rain event near rocks. Increased moisture availability would be extremely beneficial for Lake Mills revegetation (Chenoweth et al., 2011).

In addition to reducing the limitations of these models as described above, I suggest future research in testing and modeling vegetation's reaction to the manipulated microclimate and measuring long-term effects of manipulated microclimate on overall restoration success. Much is known about plant responses to varying microclimate (Kalma and Kuiper, 1966; Haeussler et al., 1995; Machado and Paulsen, 2001; Niinemets and Valladares, 2006; Peters et al., 2008; Jajarmi, 2009; Niinemets, 2010; Jones, 2013; Pastur et al., 2014). However, it would be most helpful to estimate or predict vegetation success based on these changes in microclimate around LWD. This information would provide a more concrete understanding of the benefits of LWD for

plant restoration uses. There are many studies investigating species-specific microclimate preferences. Many of these studies are about domesticated species important for agricultural use (Kalma and Kuiper, 1966; Machado and Paulsen, 2001; Jajarmi, 2009), and many others concern wild species (Haeussler et al., 1995; Niinemets and Valladares, 2006; Peters et al., 2008; Niinemets, 2010; Pastur et al., 2014). However, microclimate preferences are not known for all life stages of all Elwha watershed species. Species-specific microclimate preference information, especially for seedling stages of those species, would help better predict species-specific success with altered microclimate.

With microclimate models that are broader in scope and with more information about potential native species' reactions to manipulated microclimate, these models, or LWD microclimate manipulation models created with a similar strategy could be used to predict the impact of using LWD in a wider range of restoration sites. These models could also potentially be used to quantify and compare modification of microclimate near other barrier objects, such as walls, hedge-fences, individual plants or topographic features by using this modeling strategy.

3.8 Conclusions

This study compared the microclimates on the south, leeward, unshaded and the north, windward, shaded sides of logs on newly exposed lake sediments during late summer. The spatial pattern of microclimate in the vicinity of a log differs with direction and varies among the microclimate variables. Maximum wind speed at 10 cm height (u_{10}) was 50% less on the south side than the north side of a log exposed to wind. There was a 83% decrease in wind speed within 50 cm of the log on both the south and north sides. Maximum sediment temperature was similar on the south and north sides. Sediment temperature decreased by 10.7 ^{o}C within 72 cm of the log on its north side on average, but it was not influenced by the log on its south side. Maximum evaporation was similar on the south and north sides. Evaporation rate

decreased by 41% within 52.5 cm of the log on the north side, but was not influenced by the log on the south side.

The spatial patterns of each microclimate variable remain approximately the same with time of day and with the added variable of different days, but the ranges of the values of those variables vary.

Within a single day and over nine other days measured at varying times, maximum u_{10} ranged from 0.49 to 3.2 m/s, maximum sediment temperature from 15.5 to 43.4 ^{o}C and maximum evaporation from 26.7 to 130 mg/min. The magnitude and spatial extent of the influence of the log on microclimate also varied.

Weather and other environmental factors influenced each microclimate variable. For a repeatedly measured log that was exposed to north winds, the u_{10} to both the north and south of the log was a function of average wind speed at 1 m height ($\bar{u}_{100}$) and distance from the log, but not recent solar radiation, as initially hypothesized (Table 3.11). The T_S to the north and south were functions of air temperature and solar radiation; T_S to the north was also affected by distance from the log. The E to the north and south are functions of vapor pressure deficit and solar radiation, but not local wind speed or air temperature as originally hypothesized. The E to the north was also affected by distance from the log.

Irrespective of whether a log was exposed to north wind or protected from it, southern u_{10}, and northern T_S and E behave similarly around all logs measured. In contrast, northern u_{10}, and southern T_S and E models differed between exposed and protected logs. The models for exposed and protected logs had the same environmental factors but differed in the magnitudes of their effects, as indicated by different model coefficients (Table 3.11). This suggests that the northernmost, exposed log has a unique role in manipulating microclimate in the log-drop area.

Table 3.11: Environmental factors within each microclimate model of exposed (repeated log) and protected (other log) models. Exposed and protected log models contained the same environmental factors, but north 10 cm wind speed, south sediment temperature and south evaporation rate differed in the coefficients of those factors within their models. Surface wind speed was measured as wind speed at 10 cm height. Solar radiation includes all recent solar radiation variables. An X indicates the environmental factor is in the model.

		Environmental Factors in Model					
Microclimate Variable	**Direction**	*Solar radiation*	*Local wind speed*	*Vapor pressure deficit*	*Air temperature*	*Distance from log*	**Model coefficients of exposed vs protected logs**
Surface							
Wind Speed	North		X			X	different
	South		X			X	same
Sediment							
Temperature	North	X			X	X	same
	South				X		different
Evaporation							
Rate	North	X		X		X	same
	South	X		X			different

To the immediate north (windward) and south (leeward) of a log, u_{10} is slowed and may reduce wind stress on plants from dessication and mechanical damage. To the immediate north a log, T_S is decreased and may reduce the risk of heat damage to plant tissues and allow for more ideal metabolic rates (Jones, 2013). The E is also most reduced immediately to the north of logs. This 41% decrease in evaporative demand would likely reduce evaporation stress on plants and allow for better sediment or soil moisture retention in this area.

Placement of large woody debris is important for the Elwha restoration if the manipulated microclimate around logs allows plants to establish and survive in patches where they would not otherwise survive. Established plants nearby to logs can also manipulate microclimate and provide seeds to recruit even more vegetation. As more vegetation establishes, these once bare and inhospitable sediments on the Lake Mills valley-bottom can begin to become more similar to the forests that surround them.

The most important next step in this research is to improve the reliability of these models with other data and especially to validate the other log-derived models created in this study. Additional data from other seasons and weather conditions within the October 2014 log drop area within Lake Mills would greatly improve the applicability of this model inside this restoration area by broadening the temporal scope.

Bibliography

Adeniyi, M., and E. Nymphas. 2011. Estimation of bare soil surface temperature from air temperature and soil depth temperature in a tropical station. International Journal of Natural and Applied Sciences 7:429–437.

Ahrens, C. D. 2005. Essentials of Meteorology. Thomson Learning.

American Rivers. 2014. American Rivers dam removal database. Available online at: https://www.americanrivers.org/threats-solutions/restoring-damaged-rivers/ Accessed: April 20, 2017.

Armas, C., S. Rodríguez-Echeverría, and F. I. Pugnaire. 2011. A field test of the stress-gradient hypothesis along an aridity gradient. Journal of Vegetation Science 22:818–827.

Aronson, J., J. Kigel, A. Shmida, and J. Klein. 1992. Adaptive phenology of desert and Mediterranean populations of annual plants grown with and without water stress. Oecologia 89:17–26.

Auble, G. T., P. B. Shafroth, M. L. Scott, and J. E. Roelle. 2007. Early vegetation development on an exposed reservoir: implications for dam removal. Environmental Management 39:806–818.

Bang, C., J. L. Sabo, and S. H. Faeth. 2010. Reduced wind speed improves plant growth in a desert city. PLoS One 5:e11061.

Bellmore, J. R., J. J. Duda, L. S. Craig, S. L. Greene, C. E. Torgersen, M. J.

Collins, and K. Vittum. 2017. Status and trends of dam removal research in the United States. Wiley Interdisciplinary Reviews: Water 4.

Bertness, M. D., and R. Callaway. 1994. Positive interactions in communities. Trends in Ecology & Evolution 9:191–193.

Blood, L. E., and J. H. Titus. 2010. Microsite effects on forest regeneration in a bottomland swamp in western New York. The Journal of the Torrey Botanical Society 137:88–102.

Brandle, J. R., X. Zhou, and L. Hodges. 2006. How windbreaks work. The Board of Regents of the University of Nebraska on behalf of the University of Nebraska - Lincoln Extension. Available online at: http://extensionpublications.unl.edu/assets/pdf/ec1763.pdf. Accessed: May 30, 2018.

Butterfield, B. J., J. B. Bradford, C. Armas, I. Prieto, and F. I. Pugnaire. 2016. Does the stress-gradient hypothesis hold water? Disentangling spatial and temporal variation in plant effects on soil moisture in dryland systems. Functional Ecology 30:10–19.

Chen, J., J. F. Franklin, and T. A. Spies. 1995. Growing-season microclimatic gradients from clearcut edges into old-growth douglas-fir forests. Ecological Applications 5:74–86.

Chen, J., S. C. Saunders, T. R. Crow, R. J. Naiman, K. D. Brosofske, G. D. Mroz, B. L. Brookshire, and J. F. Franklin. 1999. Microclimate in forest ecosystem and landscape ecology variations in local climate can be used to monitor and compare the effects of different management regimes. BioScience 49:288–297.

Chenoweth, J., S. A. Acker, and M. L. McHenry. 2011. Revegetation and restoration plan for Lake Mills and Lake Aldwell. Olympic National Park and the Lower Elwha Klallam Tribe. Port Angleles, WA.

Cook, F. J., and V. A. Orchard. 2008. Relationships between soil respiration and soil moisture. Soil Biology and Biochemistry 40:1013–1018.

Covell, S., R. Ellis, E. Roberts, and R. Summerfield. 1986. The influence of temperature on seed germination rate in grain legumes i. a comparison of chickpea, lentil, soyabean and cowpea at constant temperatures. Journal of Experimental Botany 37:705–715.

David, Ř., K. Tomáš, K. Josef, V. Jan, and P. Martin. 2016. The character of windbreaks and their influence on mitigation of soil erosion. Bulletin of the Faculty of Forestry/Glasnik Sumarskog fakulteta 114.

Davies-Colley, R. J., G. Payne, and M. Van Elswijk. 2000. Microclimate gradients across a forest edge. New Zealand Journal of Ecology 24:111–121.

Fryrear, D. W., and E. Skidmore. 1985. Methods for controlling wind erosion. Chap. 24, pages 443–457 *in* R. F. Follett and B. A. Stewart, eds. Soil Erosion and Crop Productivity. ASA-CSSA-SSSA, Madison, WI.

Gehlhausen, S. M., M. W. Schwartz, and C. K. Augspurger. 2000. Vegetation and microclimatic edge effects in two mixed-mesophytic forest fragments. Plant Ecology 147:21–35.

Geiger, R., R. H. Aron, and P. Todhunter. 2009. The Climate Near the Ground. 7th ed. Rowman & Littlefield, Landham, MD.

Grace, J. 1977. Plant Response to Wind. Academic Press., New York.

Gray, A. N., and T. A. Spies. 1997. Microsite controls on tree seedling establishment in conifer forest canopy gaps. Ecology 78:2458–2473.

Gray, A. N., T. A. Spies, and M. J. Easter. 2002. Microclimatic and soil moisture responses to gap formation in coastal Douglas-fir forests. Canadian Journal of Forest Research 32:332–343.

Grier, C. C. 1988. Foliage loss due to snow, wind, and winter drying damage: its effects on leaf biomass of some western conifer forests. Canadian Journal of Forest Research 18:1097–1102.

Haeussler, S., J. C. Tappeiner II, and B. J. Greber. 1995. Germination, survival, and early growth of red alder seedlings in the central coast range of oregon. Canadian Journal of Forest Research 25:1639–1651.

Harte, J., M. S. Torn, F.-R. Chang, B. Feifarek, A. P. Kinzig, R. Shaw, and K. Shen. 1995. Global warming and soil microclimate: Results from a meadow-warming experiment. Ecological Applications 5:132–150.

Heck, R. H., S. L. Thomas, and L. N. Tabata. 2013. Multilevel and longitudinal modeling with IBM SPSS. Routledge.

Heisler, G. M., and D. R. Dewalle. 1988. 2. Effects of windbreak structure on wind flow. Agriculture, Ecosystems & Environment 22:41–69.

Holmgren, M., and M. Scheffer. 2010. Strong facilitation in mild environments: the stress gradient hypothesis revisited. Journal of Ecology 98:1269–1275.

Idso, S. B., R. D. Jackson, and R. J. Reginato. 1978. Extending the "degree day" concept of plant phenological development to include water stress effects. Ecology 59:431–433.

Jajarmi, V. 2009. Effect of water stress on germination indices in seven wheat cultivar. World Acad. Sci. Eng. Technol 49:105–106.

Jassal, R. S., T. A. Black, D. L. Spittlehouse, C. Brümmer, and Z. Nesic. 2009. Evapotranspiration and water use efficiency in different-aged Pacific Northwest Douglas-fir stands. Agricultural and Forest Meteorology 149:1168–1178.

Jo, I., J. D. Fridley, and D. A. Frank. 2017. Invasive plants accelerate nitrogen cycling: evidence from experimental woody monocultures. Journal of Ecology 105:1105–1110.

Jones, H. 1999. Physicochemical and Environmental Plant Physiology. Journal of Applied Ecology 36:1076–1077.

Jones, H. G. 2013. Plants and microclimate: a quantitative approach to environmental plant physiology. Cambridge University Press, New York.

Kalma, J. D., and F. Kuiper. 1966. Transpiration and growth of Phaseolus vulgaris L. as affected by wind speed. Mededelingen Landbouwhogeschool, Wegeningen, Nederland.

Kearney, M., and W. Porter. 2009. Mechanistic niche modelling: combining physiological and spatial data to predict species' ranges. Ecology Letters 12:334–350.

Kearney, M. R., and W. P. Porter. 2017. Nichemapr–an r package for biophysical modelling: the microclimate model. Ecography 40:664–674.

Kim, S., J. Shiri, O. Kisi, and V. P. Singh. 2013. Estimating daily pan evaporation using different data-driven methods and lag-time patterns. Water Resources Management 27:2267–2286.

Kupferschmid, A. D., and H. Bugmann. 2005. Effect of microsites, logs and ungulate browsing on Picea abies regeneration in a mountain forest. Forest Ecology and Management 205:251–265.

Larjavaara, M., and H. C. Muller-Landau. 2010. Comparison of decay classification, knife test, and two penetrometers for estimating wood density of coarse woody debris. Canadian Journal of Forest Research 40:2313–2321.

Likso, T., and K. Pandžić. 2006. Diurnal variation of air temperature in the atmospheric surface layer. Agriculturae Conspectus Scientificus 71:87–93.

Lortie, C. J., and R. M. Callaway. 2006. Re-analysis of meta-analysis: support for the stress-gradient hypothesis. Journal of Ecology 94:7–16.

Machado, S., and G. M. Paulsen. 2001. Combined effects of drought and high temperature on water relations of wheat and sorghum. Plant and Soil 233:179–187.

Maestre, F. T., R. M. Callaway, F. Valladares, and C. J. Lortie. 2009. Refining the stress-gradient hypothesis for competition and facilitation in plant communities. Journal of Ecology 97:199–205.

Maestre, F. T., F. Valladares, and J. F. Reynolds. 2006. The stress-gradient hypothesis does not fit all relationships between plant–plant interactions and abiotic stress: further insights from arid environments. Journal of Ecology 94:17–22.

Mayaud, J. R., G. F. Wiggs, and R. M. Bailey. 2016. Characterizing turbulent wind flow around dryland vegetation. Earth Surface Processes and Landforms 41:1421–1436.

McHenry, M., and J. Chenoweth. 2015. Revegetation of the Former Mills Reservoir on the Elwha River Following Dam Removal: Moving Large Wood by Helicopter to Assist Revegetation Efforts. Available online at http://blogs.nwifc.org/psp/files/2015/02/Mills-Reservoir-Helicopter-LWD -Projects-022815.pdf .

McMichael, B., and J. Burke. 1996. Temperature effects on root growth. Plant roots: The hidden half 2:383–396.

Michel, J. T., J. M. Helfield, and D. U. Hooper. 2011. Seed rain and revegetation of exposed substrates following dam removal on the elwha river. Northwest Science 85:15–29.

Middleton, B. 1999. Wetland restoration, flood pulsing, and disturbance dynamics. John Wiley & Sons.

Middleton, B. 2000. Hydrochory, seed banks, and regeneration dynamics along the landscape boundaries of a forested wetland. Plant Ecology 146:167–181.

Monteith, J., and M. Unsworth. 2007. Principles of Environmental Physics. Academic Press.

Monteith, J. L., and M. H. Unsworth. 1990. Principles of environmental physics, edited by: Arnold. SE, London, UK .

Morse, R., and L. Evans. 1962. Design and development of CERES-an Australian phytotron. CSIRO. Division of Mechanical Engineering.

Mutiibwa, D., S. Strachan, and T. Albright. 2015. Land surface temperature and surface air temperature in complex terrain. IEEE Journal of Selected Topics in Applied Earth Observations and Remote Sensing 8:4762–4774.

Newmark, W. D. 2001. Tanzanian forest edge microclimatic gradients: dynamic patterns 1. Biotropica 33:2–11.

Niinemets, Ü. 2010. Responses of forest trees to single and multiple environmental stresses from seedlings to mature plants: past stress history, stress interactions, tolerance and acclimation. Forest Ecology and Management 260:1623–1639.

Niinemets, Ü., and F. Valladares. 2006. Tolerance to shade, drought, and waterlogging of temperate Northern Hemisphere trees and shrubs. Ecological Monographs 76:521–547.

Palace, M., M. Keller, G. P. Asner, J. N. M. Silva, and C. Passos. 2007. Necromass in undisturbed and logged forests in the Brazilian Amazon. Forest Ecology and Management 238:309–318.

Pastur, G. J. M., R. S. Esteban, J. M. Cellini, M. V. Lencinas, P. L. Peri, and M. G. Neyland. 2014. Survival and growth of Nothofagus pumilio seedlings under several microenvironments after variable retention harvesting in southern Patagonian forests. Annals of Forest Science 71:349–362.

Penman, H. L. 1948. Natural evaporation from open water, bare soil and grass. Pages 120–145 *in* Proceedings of the Royal Society of London A: Mathematical, Physical and Engineering Sciences. Vol. 193. The Royal Society.

Peters, E. M., C. Martorell, and E. Ezcurra. 2008. Nurse rocks are more important than nurse plants in determining the distribution and establishment of globose cacti (Mammillaria) in the Tehuacán Valley, Mexico. Journal of Arid Environments 72:593–601.

Phillips, E. L., and W. R. Donaldson. 1972. Washington climate for Clallam, Grays Harbor, Jefferson, Pacific, and Wahkiakum Counties. Cooperative Extension Service Publication EM 3708. Washington State University. Pullman, Washington .

Questad, E. J., J. R. Kellner, K. Kinney, S. Cordell, G. P. Asner, J. Thaxton, J. Diep, A. Uowolo, S. Brooks, N. Inman-Narahari, et al. 2014. Mapping habitat suitability for at-risk plant species and its implications for restoration and reintroduction. Ecological Applications 24:385–395.

Raich, J. W., and A. Tufekciogul. 2000. Vegetation and soil respiration: correlations and controls. Biogeochemistry 48:71–90.

Randle, T. J., J. A. Bountry, A. Ritchie, and K. Wille. 2015. Large-scale dam removal on the Elwha River, Washington, USA: Erosion of reservoir sediment. Geomorphology 246:709–728.

Rosenberg, N. J., B. L. Blad, and S. B. Verma. 1983. Microclimate: the biological environment. John Wiley & Sons.

Schuster, J. L. 2015. Vegetation colonization within exposed reservoirs following dam removal on the Elwha River, Washington. M.S. Thesis Eastern Washington University .

Shuttleworth, W. J. 1993. Evaporation. Chap. 4, pages 4.1–4.53 *in* D. R. Maidment, ed. Handbook of Hydrology. McGraw-Hill, New York.

Skidmore, E., and L. Hagen. 1973. Potential evaporation as influenced by barrier-induced microclimate. Pages 237–244 *in* Physical Aspects of Soil Water and Salts in Ecosystems. Springer-Verlag Berlin Heidelberg, A. Hadas, D. Swartzendruber, P. E. Rijtema, M. Fuchs and B. Yaron.

Stanford, J. A., J. Ward, W. J. Liss, C. A. Frissell, R. N. Williams, J. A. Lichatowich, and C. C. Coutant. 1996. A general protocol for restoration of regulated rivers. Regulated Rivers: Research & Management 12:391–413.

Stanley, E. H., and M. W. Doyle. 2003. Trading off: the ecological effects of dam removal. Frontiers in Ecology and the Environment 1:15–22.

Supuka, J., and P. Uhrin. 2016. Share of scattered woody vegetation in landscape ecological stability and agriculture sustainability. Folia Oecologica 43:193.

Swinbank, W. 1964. The exponential wind profile. Quarterly Journal of the Royal Meteorological Society 90:119–135.

Tabari, H., S. Marofi, and A.-A. Sabziparvar. 2010. Estimation of daily pan evaporation using artificial neural network and multivariate non-linear regression. Irrigation Science 28:399–406.

Tan, C., and T. Black. 1976. Factors affecting the canopy resistance of a douglas-fir forest. Boundary-Layer Meteorology 10:475–488.

Tennekes, H. 1973. The logarithmic wind profile. Journal of the Atmospheric Sciences 30:234–238.

Tullos, D. D., M. J. Collins, J. R. Bellmore, J. A. Bountry, P. J. Connolly, P. B. Shafroth, and A. C. Wilcox. 2016. Synthesis of common management concerns associated with dam removal. JAWRA Journal of the American Water Resources Association 52:1179–1206.

Turner, M. G. 1989. Landscape ecology: the effect of pattern on process. Annual Review of Ecology and Systematics 20:171–197.

Wadsworth, R. 1959. An optimum wind speed for plant growth. Annals of Botany 23:195–199.

Wahid, A., S. Gelani, M. Ashraf, and M. R. Foolad. 2007. Heat tolerance in plants: an overview. Environmental and Experimental Botany 61:199–223.

Walker, L. R., and R. Del Moral. 2003. Primary succession and ecosystem rehabilitation. Cambridge University Press.

Waring, R. H., and J. F. Franklin. 1979. Evergreen coniferous forests of the Pacific Northwest. Science 204:1380–1386.

Winter, B. D., and P. Crain. 2008. Making the case for ecosystem restoration by dam removal in the Elwha River, Washington. Northwest Science 82:13–28.

Woodruff, N. P., L. Lyles, and D. Fryrear. 1963. Reducing wind velocity with field shelterbelts, vol. 131. Agricultural Experiment Station, Kansas State University of Agriculture and Applied Science.

Xu, M., Y. Qi, J. Chen, and B. Song. 2004. Scale-dependent relationships between landscape structure and microclimate. Plant Ecology 173:39–57.

Appendix A

Exposure time and evaporation rate

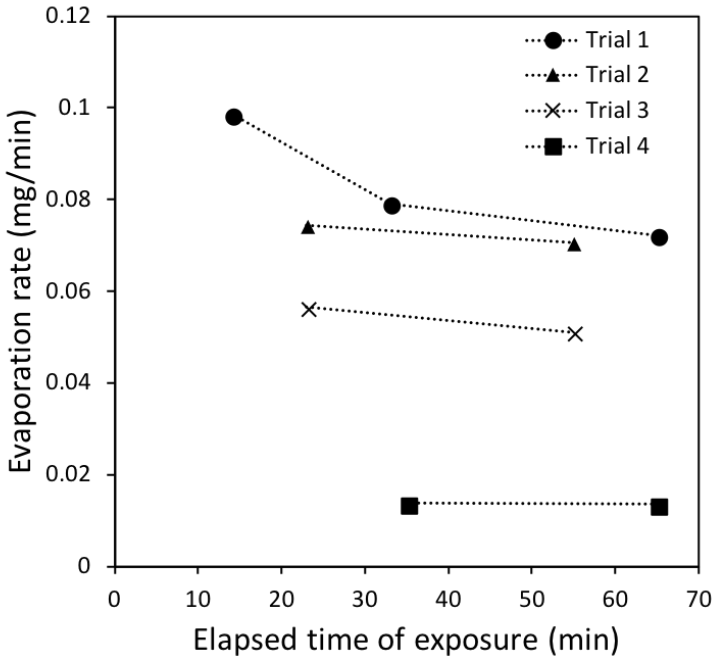

Figure A.1: Evaporation rate versus exposure time. Trials 1, 2 and 3 were measured on July 19, 2015. Clear sky, sunny, approximately 30 ^{o}C, slight breeze. Trial 4 was measured on July 24, 2015, weather was partially cloudy, approximately 15^{o}C with a slight breeze. Trials 1 and 2 were measured in full sun. Trials 3 and 4 were exposed in shade. Evaporation rate was measured gravimetrically from tennis balls.

Appendix B

Roughness distance (z_0)

Concept and Calculation

The z_0 describes the height at which wind speed becomes negligble. In this study, z_0 is used to describe the affect LWD has on wind speed and turbulence nearby. Higher z_0 values indicate wind is slowed relative to the overall wind pattern at higher vertical distances at a single point, likely caused by increased surface roughness. Lower z_0 values indicate that the wind speed is more similar to the wind speed at a greater vertical distance and is less affected by ground surface friction.

$$u = \frac{u^*}{k} ln \frac{z}{z_0}$$

where u is the wind speed in cm/sec, u^* is the friction velocity (cm/sec), k is the von Karman's constant, z is the height above the ground level in cm, and z_0 is 'roughness distance' (Rosenberg et al., 1983; Jones, 2013) (Figure 1.1).

I used the wind profile equation described above to solve for z_0

$$z_0 = e^{ln(z_1) - \frac{ln(z_2) - ln(z_1)}{u_2 - u_1} u_1}$$

where z_1 and z_2 are two different heights in meters and u_1 and u_2 are wind speeds (in meters per second (m/s)) at heights z_1 and z_2, respectively.

The u at 10 cm and 100 cm heights at each distance from the log were used to calculate z_0 from the equation above (See section 2.5.1 for u measurement methods).

Known height (10 cm and 100cm) and u measurements can be used to calculate m and b with $m = \frac{lnz_2 - lnz_1}{u_2 - u_1}$ and $b = lnz_1 - mu_1$. The roughness parameter z_0 can then be calculated by $z_0 = e^b$. The u_1 and u_2 are the u (m/s) at the two heights z_1 and z_2 (m), respectively.

The u_1 predicted in these models are constrained by the minimum possible u of 0 m/s and u_2. Therefore, a lower u_2 increases the probability that u_1 is more similar to u_2 . In these instances, z_0 would be lower and wind effects of logs would not be detected as easily.

Results and Discussion

Within-day variability When distance appeared to have an effect on z_0, the greatest z_0 values occurred nearest to the log at all times to both the north (windward) and south (leeward) (Figure B.1). At 9:28 to both the north and south, 17:06 north and 11:30 south, distance from the log was not related to z_0. To the north, the wind is redirected upwards and over the log, creating a region with lowered u, indicated by greater z_0 values. This region extends approximately 50 cm to 75 cm to the north on August 21, 2015.

To the south (lee), the roughness distance remains greater than 0.01 cm at greater distances, unlike to the north where z_0 approaches 0.01 to 0 at distances greater than

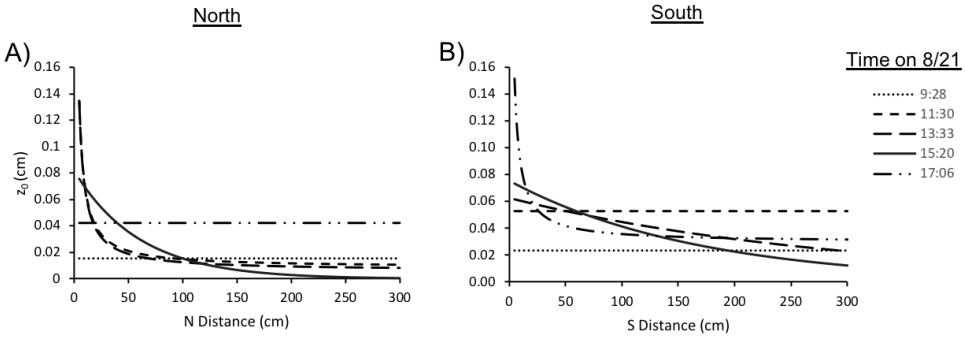

Figure B.1: Selected curves to represent transects for 5 measured times of day on August 21, 2015. A represents transects measured to the north of the repeated log and B represents transects measured to the south of the repeated log. Both A and B both contain a single line generated for that transect at 9:28, 11:30, 13:33, 15:20 and 17:06 measured times.

150 cm. This means that the log decreases horizontal wind velocity on the leeward side for greater than 300 cm, which is approximately four times the height of the log. Mayaud et al. (2016) describes decreased wind velocity for a distance up to nine times the height of the barrier object, so this result may be reasonable. This elevated z_0 may reduce mechanical wind stress on plants, and might lessen the evaporative stress on plants to the south of logs (Grace, 1977).

The lack of a pattern between z_0 modeled to the north and the south indicates that the log's effect on z_0 is variable. At 9:28, the z_0 to the north and the south behave approximately the same and distance has no effect. However, at 17:06, the distance from the log to the north has no effect on z_0, but there is a relationship between distance and z_0 to the south. This pattern is opposite for 11:30.

Among-day Variability The z_0 patterns on different days were similar to the z_0 regression in the within-day analysis. Adding the varying days during the study as a variable to the different times of day, increases the range of results seen in roughness distance. This suggests that the values of z_0 are affected by both time of day and day during this study.

To the south among days, z_0 patterns appear similar to the single-day z_0. These show increased z_0 values within 50 cm of the log and show a minimum z_0 value of 0.020 cm (Figures B.1 B and B.2 B). Similar to the within-day regressions, the among-day regressions to the south do not drop to the minimum value modeled to the north (less

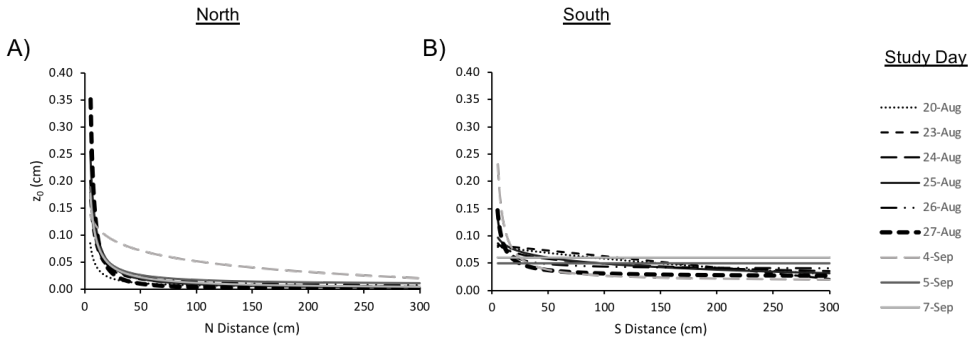

Figure B.2: The z_0 measured along transects of the repeat log each study day. Graph A represents transects measured to the north of the repeated log and B represents transects measured to the south of the repeated log.

than 0.010 cm), but show z_0 greater than 0.020 cm to the south,extending greater than 300 cm, reducing mechanical and evaporative wind stress on plants (Grace, 1977) (Figure B.2).